Ocean Engineering 219 (2021) 108377

Contents lists available at ScienceDirect

Ocean Engineering

journal homepage: www.elsevier.com/locate/oceaneng

Design and comparative analysis of alternative mooring systems for floating wind turbines in shallow water with emphasis on ultimate limit state design

Kun Xu [a,f,*], Kjell Larsen [a,b,c], Yanlin Shao [d,e], Min Zhang [f], Zhen Gao [a,b], Torgeir Moan [a,b]

[a] Department of Marine Technology, Norwegian University of Science and Technology (NTNU), Trondheim, 7491, Norway
[b] Centre for Autonomous Marine Operations and Systems (AMOS), NTNU, Trondheim, 7491, Norway
[c] Equinor ASA, Arkitekt Ebbells Veg 10, Ranheim, 7053, Norway
[d] Department of Mechanical Engineering, Technical University of Denmark, 2800, Kgs. Lyngby, Denmark
[e] Shipbuilding Engineering Institute, Harbin Engineering University, 150001, Harbin, China
[f] Shandong Provincial Key Lab of Ocean Engineering, Ocean University of China, Qingdao, 266100, China

ARTICLE INFO

Keywords:
Floating wind turbine
Shallow water
Hybrid mooring design
Synthetic fibre rope
Syrope model

ABSTRACT

Floating wind turbines represent a cost-efficient energy solution in deep water where bottom-fixed wind turbine becomes excessively expensive. However, mooring design is quite challenging for all shallow water depths including the transition water depth between bottom-fixed and floating wind turbines, in the order of 50–80 m, for which floating concepts might become more cost-effective than bottom-fixed ones. In this paper, mooring system design for floating wind turbine in shallow water are studied considering both catenary and taut mooring systems. Seven mooring concepts designed for a 5 MW semi-submersible floating wind turbine at 50 m water depth are compared with the purpose to identify solutions that are structurally reliable and economically attractive. The concepts are made of different mooring line materials (chain and synthetic fibre rope), mooring components (clump weight and buoy) and anchors (drag embedment anchor and suction anchor). Based on the latest experimental data, the nonlinear tension-dependent stiffness of synthetic fibre rope are described with an improved numerical model. Performance of the seven mooring concepts are compared with respect to mooring line characteristics, motion response amplitude operator, utilization factor considering the ultimate limit state design and cost etc. Six mooring design concepts are finally recommended for future assessment regarding the application of floating wind turbines in shallow water say 50 m and deeper.

1. Introduction

Wind energy is characterized as clean and reliable power and it has experienced a rapid development in recent years in both onshore and offshore sectors (Global Wind Energy Council, 2019). Compared with onshore wind, several attributes for offshore wind make its future quite promising such as immense stable resource, great area availability, easy transportation, little visual disturbance and noise etc.

Offshore wind resources in many countries is found at a water depth above 50 m where bottom fixed wind turbine becomes less cost-attractive and floating wind turbine is considered as a better alternative (Myhr et al., 2014). As the world's first floating wind farm in operation, Hywind Scotland which consists of five 6 MW Hywind spars was commissioned in October 2017. In August 2019, Hywind Tampen project (Equinor, 2020) was launched with the purpose of supplying power to the Snorre and Gullfaks oil fields from 2022. Meanwhile, semi-submersible floating wind turbine started to make a figure recently taking advantage of its smaller draft and wider range of applicable water depth. It has been successfully implemented in the world's second floating wind farm - WindFloat Atlantic in Portugal which consists of three 8.4 MW WindFloat semi-submersibles (edp renewable, 2020). The WindFloat concept was also implemented in the 50 MW Kincardine offshore wind farm in UK which features a total of five 9.525 MW turbines and one 2 MW turbine. The 2 MW turbine was connected to British grid in October 2018 (NS ENERGY, 2020). The manufacturing work of the remaining five WindFloat foundations began in March 2019 at the Navantia Fene yard in Spain and three foundations have been assembled by March 2020 while all five foundations are expected to be ready and delivered by summer 2020 (4COffshore, 2020).

Despite all the progress, there are still some challenges that remain to

* Corresponding author. Department of Marine Technology, Norwegian University of Science and Technology (NTNU), Trondheim, 7491, Norway..
E-mail addresses: kun.xu@ntnu.no, xukun@ouc.edu.cn (K. Xu).

https://doi.org/10.1016/j.oceaneng.2020.108377
Received 25 May 2020; Received in revised form 29 September 2020; Accepted 10 November 2020
Available online 25 November 2020

Table 1
Properties of OC4 and Bluewhale I (The mass for OC4 includes the platform and wind turbine.).

	OC4[a]	Bluewhale I[b]
Length × Width*Height (m)	74 × 67.3*120	117 × 92.7*118
Total mass (t)	14 040	43 725
Displacement (t)	13 986	69 768

[a] For a 5 MW wind turbine, 14 000 t displacement is on the upper limit of the size of a steel support structure. A typical size for the 5 MW wind turbine is between 5000 t and 7000 t, while a floater with displacement of 14 000 t could support a 15 MW wind turbine by referring to the properties of IEA 15 MW reference wind turbine (Gaertner et al., 2020).

[b] Generally, for modern steel drilling semi-submersibles in ultra-deep water, the displacements are in the range between 25 000 t to 30 000 t or higher, while the displacement for floating production platforms are even larger.

be solved before floating wind turbine can be further promoted with bigger market. One of them is the design of mooring system for a water depth of about 50 m–80 m which is normally considered as the transition water depth between floating and bottom-fixed wind turbines. When water depth becomes shallow, the effective water depth from fairlead to seabed for the mooring system to function becomes quite limited, which makes the mooring design more challenging than that in deep water. Despite rich experience of mooring design in offshore oil & gas industry, the design requirement and consideration between large oil & gas platform and floating wind turbine are quite different:

- The size of a typical floating oil and gas platform normally is much larger than floating wind platform considering the dimensions, mass, displacement etc. As an example, the general properties of the seventh-generation semi-submersible drilling platform – Bluewhale I and the OC4 semi-submersible wind turbine is compared in Table 1. For a 5 MW floating wind turbine, the displacement typically is in the range between 5000 t and 7000 t. As for the OC4 semi-submersible in this study, the displacement is close to 14 000 t while the mass of ballasting water takes significant part (9621 t). Therefore, a steel floater of 14 000 t displacement could also support a 15 MW turbine with proper ballast by referring to the properties of IEA 15 MW reference wind turbine (Gaertner et al., 2020).
- Floating wind farm normally consists of several floating units, space clearance and wake effect have to be considered when designing mooring system (Wise and Bachynski, 2020). These issues are not relevant for oil platform.
- The mean offset of floating wind turbine is greatly influenced by the thrust force at different wind speeds whose influence is quite different for oil and gas platform.
- Failure of mooring lines of manned oil and gas platforms may cause severe consequences in terms of fatalities or severe pollution while the mooring line failure consequences of floating wind turbines essentially are economical. Hence, mooring line criteria for oil and gas platforms are more restrictive, and typically including damage assessment.

The design issues of mooring system for floating wind turbine in shallow water has been investigated by several researchers. Brommundt et al. (2012) developed a numerical tool for the optimization of catenary mooring systems. A case study was performed for a semi-submersible floating wind turbine with two water depths (75 m and 330 m). The optimal line length, angle and horizontal distance between anchor and fairlead are studied. Benassai et al. (2014a) compared the motion control performance of catenary and tensioned line mooring systems for the Dutch tri-floater wind turbine at water depth between 50 m and 200 m. Both operational and extreme load cases are considered. The weight of chain cable and steel wire rope are compared at different water depths. Benassai et al. (2014b) extended the study to the influence of line number, platform maximum admissible offset and mooring line pattern. Mooring configurations consisting of nine or twelve lines were recommended. The results indicated that the mooring line weight is independent of water depth between 100 m and 200 m, while the weight will increase outside this range. Benassai et al. (2015) further investigated the mooring optimization technique from allowable platform offset, line number and mooring pattern. The results indicated that mooring weight reduction for traditional mooring configuration can be achieved by designing mooring patterns with non-uniform angular distribution. Campanile et al. (2018) proposed several catenary mooring designs for the Dutch tri-floater wind turbine at water depth from 50 m to 80 m and from 200 m to 350 m respectively. Recommendations were provided with respect to line number, platform admissible offset and minimum spacing between adjacent wind turbines etc. A preliminary cost analysis was performed regarding the installation and maintenance cost. Xu et al. (2018) proposed mooring system designs at three water depths (50 m, 100 m and 200 m) and concluded that the nonlinear mooring line tension increment becomes more significant as water depth decreases.

Use of clump weight and buoy can improve the mooring performance by balancing compliance and strength. The application of clump weight in mooring system can be traced back to 'the guyed tower' proposed by Finn (1976). In extreme conditions when the platform experiences large motions, the clump weight will be lifted from the seabed to establish an extended catenary shape to minimize the floater motion. Morrison and Asce (1983) further proved the significant resistance to horizontal loading for the guyed tower due to the attachment of clump weight. The benefit of attaching buoy to mooring line was studied by Mavrakos et al. (1996) and confirmed that the reduction of mooring line dynamics can be achieved when the size, number and location of buoy are properly selected. The study was further continued by Mavrakos and Chatjigeorgiou (1997) with frequency domain and time domain analysis. The buoy-attached mooring was applied for wave energy converter at a water depth of 50 m by Fitzgerald and Bergdahl (2007) and proved that buoy can reduce the cable weight, induced mooring loads and the influence on the floater motion. Hybrid mooring concepts consisting of both clump weight and buoy have also been developed for offshore applications. Mooring configurations consisting of catenary chain with or without additional clump weight or buoy were compared by Vicente et al. (2011) for a floating point absorber. The results showed that the maximum horizontal motion and absorbed power are less sensitive to different configurations of the buoys and clump weights than average and maximum mooring line tension. Yuan et al. (2014) developed a hybrid mooring concept for semi-submersible platform in deep water, which consists of clump weights and buoys attached to the lower and upper end of the line respectively. The performance of platform motion and line tension were improved.

The challenges of mooring system design for floating wind turbine in shallow water were considered in several industrial projects. Normally, the location of fairlead which is used to connect mooring line and floater is beneath water level. The technique of moving fairlead from underwater to above water level have been adopted by INNWIND.EU (2017) and LIFES50+ (2018) for designing floating wind turbines. The change of fairlead location artificially increases the effective water depth from fairlead to seabed, which is beneficial to improve the mooring line tension characteristics. However, one potential disadvantage is the corrosion and fatigue issues, in particular for chain links and steel wires.

Synthetic fibre ropes rather than chain links and steel wire rope are considered by more and more offshore renewable projects because of the lower weight and cost. Synthetic fibre rope mooring system was first used in offshore oil & gas industry. Petrobras pioneered the application to the P-27 platform in 1997 (Rossi et al., 2010). Ever since then, it has experienced a booming development as deep or ultra-deep water mooring solutions all over the world including Brazil, Gulf of Mexico, North sea (Bugg et al., 2004). Meanwhile, the application of synthetic fibre ropes for offshore renewable project is still at an early stage. There are only a few projects that consider synthetic fibre rope as mooring solutions, including CETO wave energy converter (Carnegie Clean

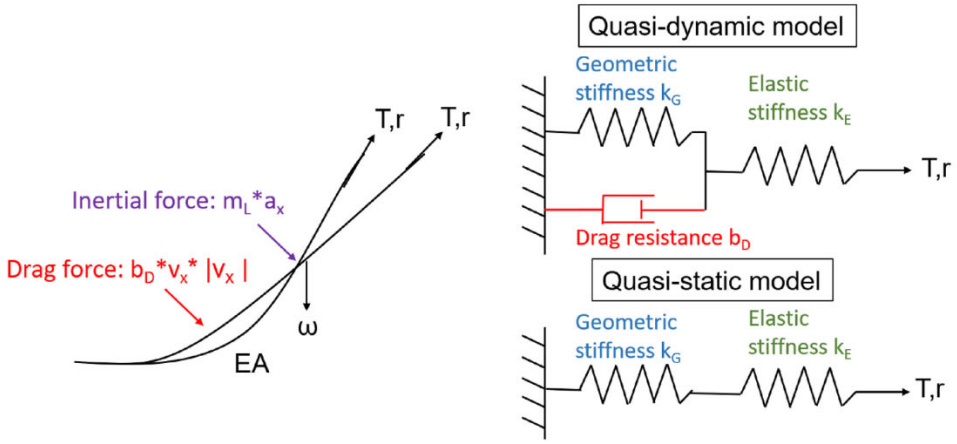

Fig. 1. Mooring system stiffness.

Energy, 2020) and Floatgen wind turbine (ideol, 2020). Weller et al. (2015) provided an overview of the application of synthetic ropes for marine renewable projects from different perspectives including classification, model testing, installation, degradation and maintenance etc.

The state-of-the-art of mooring system design for floating wind turbine in shallow water can be summarized as follows:

1. The previous mooring design studies for shallow water were mainly made of pure chain links with no clump weight or buoy included. The influence of water depth on design parameters was focused rather than sophisticated structural design at a specific water depth. The proposed hybrid mooring concepts combined with clump weights and buoys were mainly designed for deep water application and the application in shallow water mooring was not considered.
2. The experience with synthetic fibre ropes in the oil & gas sector is mainly for deep and ultra-deep water, however there is also great potential of synthetic fibre rope mooring in shallow water due to its lower elastic stiffness and capital cost.
3. The material property and the structural behavior of synthetic fibre rope is more complex than chain cable and steel wire rope. The change-in-length response of synthetic fibre rope is non-linear and load path dependent. Current industrial practice is to use the upper-bound and lower-bound method (API, 2014), which is not only conservative but also inconsistent because the offset is obtained based on a lower-bound stiffness model while the dynamic tension is estimated through another upper-bound stiffness model. There is still a lack of a well-defined understanding of the structural characteristics and mooring analysis programs with the capability to simulate the non-linear change-in-length response of the synthetic fibre ropes.
4. Regarding the mooring system of floating wind turbines, there is a lack of comparison between alternative materials and configurations for industrial guidance.

With the purpose of further expanding the applicability of floating wind turbine in shallow water, the focus of this paper is to identify the challenges and possible solutions of mooring system design for floating wind turbine when water depth approaches its marginal range (50 m). Compared with previous studies, the highlights of this paper are summarized as follows:

1. The reasons why mooring system design becomes challenging when the water depth goes from deep to shallow is systematically studied for both catenary and taut mooring systems.
2. Hybrid mooring designs with or without clump weights and buoys are compared with pure cable system in order to assess the benefit of including additional mooring components in shallow water mooring.
3. The use of synthetic fibre rope for shallow water mooring was investigated. Considering the limitation of traditional upper-bound and lower-bound method for synthetic fibre rope analysis, a refined numerical model denoted 'Syrope' defining the static and dynamic stiffness in a single model, is applied in this paper to avoid over-conservative mooring design.
4. Despite limited publicly available data, a preliminary cost analysis for different mooring concepts was performed using information from different sources.
5. Recommendation for preferable mooring designs for floating wind turbine in shallow water depth are made for industrial guidance through comparative studies of different mooring designs.

This paper is organized as follows: The mooring design challenges in shallow water for both catenary and taut mooring systems are introduced in Section 2. Design criteria are described in Section 3.1 and the refined numerical 'Syrope' model for synthetic fibre ropes is introduced in Section 3.2. The seven comparative mooring design concepts are described into detail in Section 3.3. The OC4 semi-submersible wind turbine (Robertson et al., 2014) is selected for the case study as introduced in Section 4. The performance of the designs is compared in Section 5 considering static and dynamic behavior and cost assessment. In Section 6, the preferable mooring designs are recommended for future industrial application. In this paper, the numerical simulations are carried out in SIMA (SINTEF Ocean, 2018a, b) considering both wind and wave loads and the main design rules followed are DNVGL–OS–E301 (DNVGL, 2018a) and DNVGL-ST-0119 (DNVGL, 2018b).

The focus of this paper is to compare different mooring design concepts, therefore a number of representative load cases covering serviceability limit state (SLS) and ultimate limit state (ULS) are prioritized in this paper. Meanwhile, the structural behavior of all mooring designs in fatigue limit state (FLS) and accidental limit state (ALS) will be studied in the future. In addition, wind- and wave-induced load effects are focused in this paper while the current load effect is briefly studied through one comparative extreme load case (LC9 in Table 6).

2. Mooring design challenges for shallow water conditions

Precise positioning and motion control is critical for safe operation of the floating wind turbine considering the integrity of electric power cable. For floating structures, rigid-body motions and mooring line tension are coupled, so that mooring system provides restoring effects, as well as inertial and damping effects on floater motions. Meanwhile, both static offset and dynamic motions of the floater will influence the mooring line tension. When the floater is displaced away from the equilibrium position due to environmental forces, mooring system will operate to keep the floater in position by providing restoring force. As

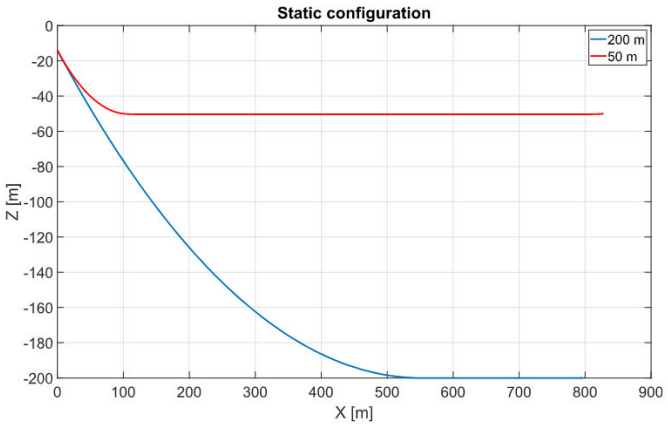

Fig. 2. Static catenary mooring configuration for the case study in this paper.

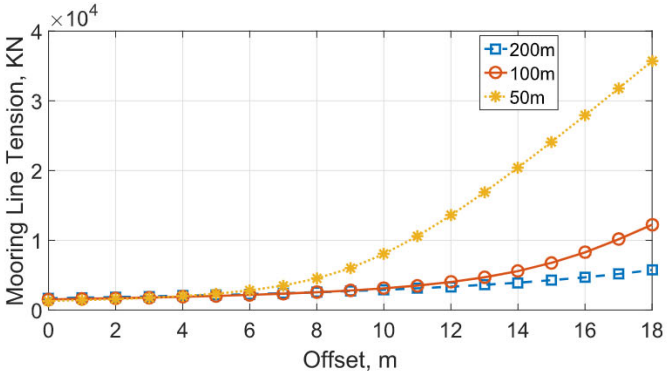

Fig. 3. Mooring line tension at 50 m, 100 m and 200 m water depth (Xu et al., 2018) (The three mooring lines are all catenary type which is made of chain cable and clump weights).

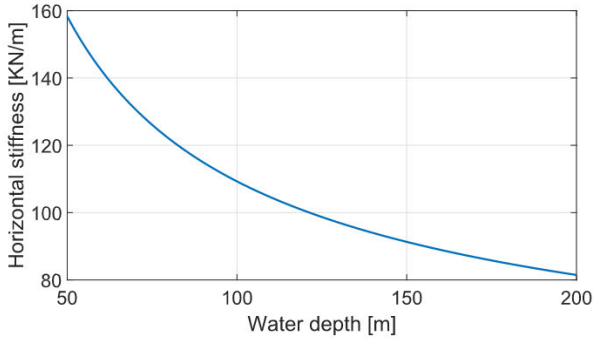

Fig. 4. Influence of water depth on horizontal mooring stiffness for the case study in this paper.

shown in Fig. 1, the total mooring restoring force (T) with respect to the fairlead motion (r) in quasi-static condition is related to geometric stiffness (k_G) and elastic stiffness (k_E). Geometric stiffness mainly comes from the weight and pre-tension of the mooring line which is the main source of restoring force in catenary mooring system. Elastic stiffness is mainly due to line elongation which is the main source of restoring force in taut mooring system with synthetic fibre rope. In dynamic conditions, mooring line motion will lead to a drag force ($b_D * v_x * |v_x|$) and an inertial force ($m_L * a_x$) which contribute to the damping and inertial effect of the mooring line, respectively. The damping effect is particularly important for floater's low frequency motions which are associated with a small potential damping. Here in the figure, b_D is drag resistance, m_L is line mass in water, v_x is line relative velocity, a_x is line acceleration, EA is axial stiffness and ω is submerged weight of the line.

Mooring system design is a complicated iterative procedure which should take into account both floater motion and mooring line tension. On one hand, the mooring system should be stiff enough to limit the floater offset under the mean wind and wave loads as well as the floater slowly-varying motions due to the second order wave loads and the wind loads. On the other hand, it should be compliant enough to allow wave-frequency floater motions and avoid large mooring line tension induced by the first order wave loads on the floater. These features are relatively easy to achieve in deep water while it is more challenging in shallow water for both catenary and taut mooring systems. The effect due to drag resistance and inertial effect of mooring line is quite limited in shallow water as studied in this paper, therefore the main design challenge is related to smart combination of the elastic and geometric stiffness.

2.1. Catenary mooring system; some aspects of geometric stiffness

The vertical span from fairlead to seabed in shallow water is much shorter than deep water as shown in Fig. 2, which directly affects the length of suspended mooring line that provides pre-tension. Taking the OC4 semi-submersible floating wind turbine (Robertson et al., 2014) in this paper as an example, the fairlead is located at 14 m below mean water level. The effective vertical distances for suspended mooring line are 36 m and 186 m when water depths are 50 m and 200 m respectively. In order to achieve reasonable pre-tension as deep water, the size of mooring line has to be increased in shallow water.

With the same x-offset increment at fairlead, longer line in shallow water will be lifted up than that in deep water. Given the same pre-tension and stiffness at zero x-offset, the mooring line tension characteristics at different water depths are provided in Fig. 3. The comparison illustrates that the mooring line stiffness increases faster with increasing x-offset for shallow water mooring than deep water mooring, meaning that if the same wave frequency motions are triggered, larger tension will be induced in shallow water mooring line. The dramatic increase in line stiffness and associated sudden increase of line tension may lead to potential line breaking. In addition, if all the mooring line parts that were originally laying on the seabed are lifted up, the stretching of the line becomes important and leads to a significant increase in stiffness and tension.

According to Faltinsen (1993), the horizontal, geometric, in-elastic stiffness k_G of a catenary mooring line can be expressed as:

$$k_G = \frac{\partial T_H}{\partial x} = \omega \left[-\frac{2}{\sqrt{1 + 2\frac{T_H}{\omega h}}} + cosh^{-1}\left(1 + \frac{\omega h}{T_H}\right) \right]^{-1} \quad (1)$$

where ω is the unit weight of mooring line, x is the horizontal offset, h is water depth and T_H is the horizontal tension. Given the same horizontal tension T_H, the horizontal stiffness increases as water depth decreases as shown in Fig. 4. The horizontal wave-frequency motions of the floating wind turbine are dominated by inertial effect. A stiffer mooring system will lead to higher natural frequencies of the horizontal motions, which are more easily excited by difference-frequency wave loads.

The top angles between mooring line and axes, α and β, indicate the level of catenary shape of mooring line as shown in Fig. 5 (a). The bigger α is and the smaller β is, the less catenary shape is left while the tighter and the more stretched the line is. The initial values for α and β at static position are determined by mooring line tightness which is influenced by the horizontal span s (distance between fairlead and touch down point), effective water depth h (distance between fairlead and seabed) and length of suspended mooring line l_s as given in Equation (2):

$$tan\beta = sinh\left(\frac{2sh}{l_s^2 - h^2}\right) \quad (2)$$

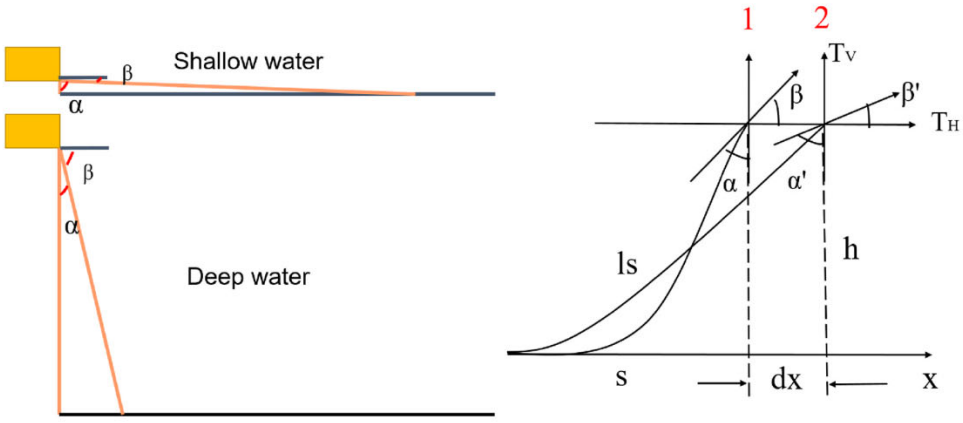

(a) Mooring line catenary shape in shallow and deep water (b) Influence of x-offset on the top angles

Fig. 5. Challenge of catenary mooring line top angles.

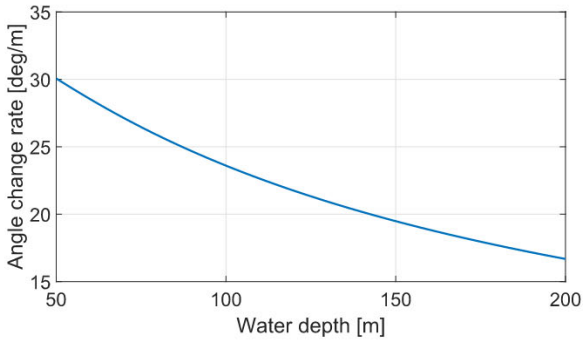

Fig. 6. The change rate of top angle α with increasing x-offsets at different water depths.

Normally deep water mooring is designed with small tightness and reasonable horizontal pre-tension can be achieved even with small angle α. This keeps a high level of catenary shape, which means it is quite rare that the mooring line will be totally stretched even for large horizontal x-offset. On the other hand, shallow water mooring is usually quite tight because the effective water depth is much smaller compared with horizontal span. In order to obtain reasonable horizontal pre-tension as deep water, the angle α has to be increased even with heavier mooring line, which as a result will eliminate certain level of catenary shape.

From dynamic perspective, the increase of x-offset at fairlead will enlarge α and decrease β, but the change rate varies at different water depths. As an example given in Fig. 5 (b), when the fairlead moves from position 1 to position 2 with a horizontal offset d_x, the angle α and β will change to α' and β'. Similar as deriving the mooring line horizontal stiffness in Equation (1), the average change rate of the angle β can be represented by the derivative of $tan\beta$ with respect to horizontal offset x:

$$\begin{aligned}\beta_x &= \frac{\mathrm{d}tan\beta}{\mathrm{d}x} = \frac{\mathrm{d}\frac{T_V}{T_H}}{\mathrm{d}x} = \frac{\frac{T_V \cdot dT_H - T_H \cdot dT_V}{(T_H)^2}}{dx} = \frac{1}{(T_H)^2}\cdot\left(T_V\cdot\frac{\mathrm{d}T_H}{\mathrm{d}x} - T_H\cdot\frac{\mathrm{d}T_V}{\mathrm{d}x}\right)\\ &= \frac{1}{(T_H)^2}\cdot\left(T_V\cdot k_G - T_H\cdot\frac{\omega\cdot \mathrm{d}l_s}{\mathrm{d}x}\right)\\ &= \frac{1}{(T_H)^2}\cdot\left(T_V\cdot k_G - T_H\cdot k_G\cdot\sqrt{\frac{1}{1+2ah}}\right)\\ &= \frac{k_G}{(T_H)^2}\cdot\left(\omega\sqrt{h^2+2ah} - T_H\cdot\sqrt{\frac{1}{1+2ah}}\right)\end{aligned} \tag{3}$$

where k_G is horizontal stiffness as described in Equation (1), ω is the unit weight of mooring line, x is the x-offset, h is water depth, a is a coefficient expressed as $a = T_H/\omega$. As a result, the average change rate for angle α expressed with unit degree can be written as:

$$\alpha_x = 90 - arctan\left(\frac{\mathrm{d}tan\beta}{\mathrm{d}x}\right) \tag{4}$$

Based on Equations (3) and (4), given the same horizontal tension T_H, the change rate of top angle, α_x, at different water depths are given in Fig. 6. The angle change rate tends to increase as water depth decreases, which means shallow water mooring is more vulnerable to lose catenary shape and be stretched to straight line than deep water mooring. It will lead to potential vertical force on the anchor which is quite dangerous. As a result, large footprint of the mooring system is normally required for shallow water with long chains laying on the seabed.

2.2. Taut mooring system; the effect of elastic stiffness

In taut mooring system, the restoring force mainly comes from the stretch of the line so that the horizontal, elastic stiffness, k_E, assuming a linearized elasticity, can be expressed as:

$$k_E = EA\frac{1}{l}sin\alpha \tag{5}$$

where E is the Young's modulus, A is the cross sectional area, l is the total line length and α is the angle between mooring line and vertical plane. Normally when water depth goes from deep to shallow, the total length of mooring line l will become shorter which will lead to a larger stiffness k_E. Therefore, when experiencing same amplitude of wave-frequency motion, the induced tension will be larger in shallow water mooring line.

Synthetic fibre rope as the most popular material used in taut mooring system is more complicated than chain and steel wire rope regarding the structural property. The nonlinear response of synthetic fibre rope is loading-path and loading-duration dependent. As shown in Fig. 7, the current industrial design practice is to use a lower-bound stiffness to calculate extreme offset and an upper-bound stiffness to calculate extreme tension. This conservative and inconsistent approach has been mentioned in several offshore standards including DNVGL-RP-E305 (DNVGL, 2015) and API-RP-2SM (API, 2014). There is a lack of comprehensive understanding of the synthetic fibre rope performance and well-established numerical program that can include the nonlinear behavior of synthetic fibre rope.

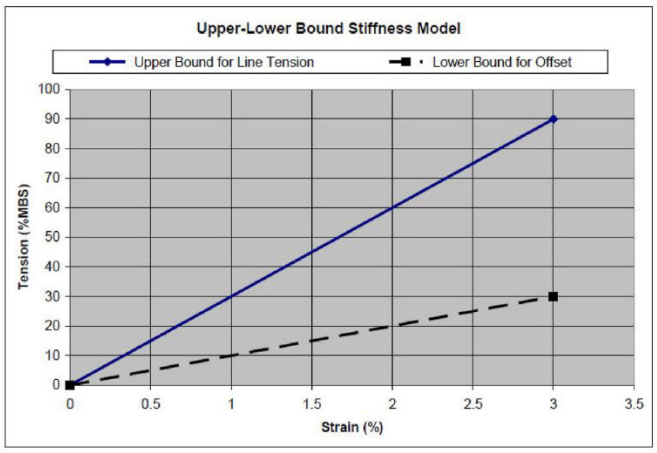

Fig. 7. Lower-bound and upper-bound stiffness model (API, 2014).

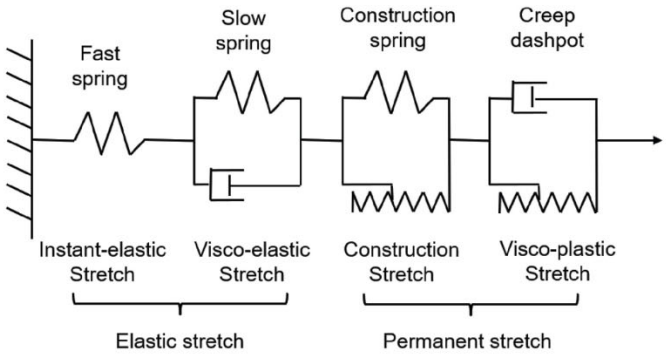

Fig. 8. The spring-dashpot model for synthetic fibre rope (Falkenberg et al., 2017).

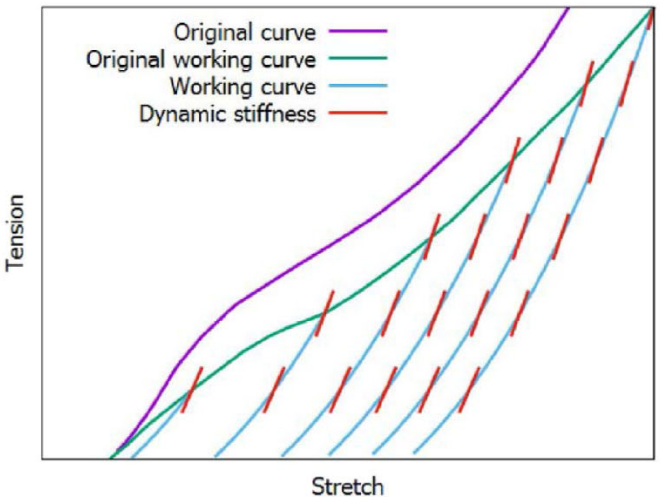

Fig. 9. 'Syrope' model (Falkenberg et al., 2017).

3. Mooring design solutions

Taking into account the design challenges mentioned in Section 2 for both catenary and taut mooring systems in shallow water, alternative mooring design concepts for floating wind turbine in shallow water e.g. about 50–80 m are investigated. The targeting water depth for the design study in this paper is chosen to be 50 m.

3.1. Design criteria

In view of the functionality of the wind turbine and the power cable, the motion characteristics of the floater and the structural safety of the mooring lines, a complete mooring design check according to DNVGL (2018a) involves ultimate limit state (ULS), fatigue limit state (FLS) and accidental limit state (ALS). In this paper, ULS design check is focused while FLS and ALS analysis will be investigated in the future. The main design criteria for shallow water mooring in this paper are:

1. Considering the safety of power cable and the power production efficiency of wind turbine, the offsets of the floater have to be limited to a reasonable range.
2. All mooring lines have to be able to withstand the load effects in all the environmental conditions considered which means that the maximum mooring line tension can not exceed the maximum breaking strength taking into account the safety factor. Fatigue damage is normally also required for a complete mooring design, but the ultimate load case is focused in this paper.
3. The catenary mooring line lying on the seabed should be long enough to avoid being totally lifted up during the lifetime and prevent drag anchor to take vertical load even in the most extreme condition.
4. The leeward mooring line should not experience slack which may lead to large snap tension.
5. The properties of a mooring system in 200 m water depth is considered as the reference for shallow water moorings. Relevant parameters are pre-tension, horizontal stiffness, line length etc.

3.2. Design basis

3.2.1. Mooring component

Clump weight is a concentrated weight which can be used to improve the geometric stiffness properties of the line. It can be incorporated with a lighter mooring line to achieve beneficial stiffness properties for the relevant top end offset.

A buoy is normally included to reduce the weight of the line, improve the geometric stiffness and provide sufficient clearance to any subsea equipment. The use of buoys in shallow water moorings could also reduce the non-linearity of the geometric stiffness and hence reduce extreme tension at large x-offsets.

3.2.2. Synthetic fibre ropes - the 'syrope' model

Many research projects have been recently launched with the objective to improve the modelling of synthetic fibre rope mooring lines. Among them, Syrope JIP (Falkenberg et al., 2017) led by DNV GL provided specific and practical guidelines based on extensive laboratory testing. In order to better describe the complex behavior of the synthetic fibre rope, a spring-dashpot model is proposed for illustration as shown in Fig. 8. The elastic stretch consists of instant-elastic and visco-elastic stretch which can be considered as a spring without and with a damper separately. The permanent stretch on the other hand includes visco-plastic stretch which is irreversible when exposed to tension and construction stretch where the ratchet allows the spring to extend above previous highest tension without retraction. In order to avoid permanent stretch, a relevant installation procedure of a synthetic fibre rope is to pre-tension/cross-tension the rope to the predicted maximum tension level it will experience during its service life. The length of the mooring line has then already reached the longest possible length and there will be no further permanent bedding-in extension (Rowley and Leite, 2011).

The 'Syrope' model as shown in Fig. 9, was proposed in the JIP (Falkenberg et al., 2017) to better describe the tension-stretch and axial stiffness characteristics for synthetic fibre rope used in mooring analysis. Based on the results from sub-rope testing, the 'Syrope' model can be interpreted as a combination of four curves:

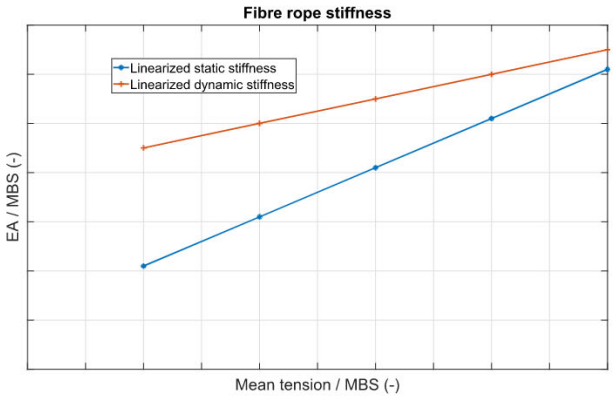

Fig. 10. Linearized static and dynamic elastic stiffness of synthetic fibre ropes. Typical curve shapes from full-scale 'Syrope' testing and internal work in Equinor (Stenlund, 2018).

- **Original curve** represents the tension-stretch relationship during the first, rapid loading of the new rope, which can be considered as the upper limit of the tension-stretch curve.
- **Original working curve** represents the stationary curve when the rope is at the mean tension with permanent stretch taken out.
- **Working curve** represents the curve when the rope is at a lower mean tension than the previous historical maximum mean tension. In a stationary sea state, the working curve is determined by the historically highest mean tension level while the exact working point on the curve is determined by the mean tension level.
- **Dynamic stiffness** represents the slope of the linearized stiffness curve for a given mean tension. It increases with mean tension and is used to calculate the tension dynamics due to low-frequency (LF) and wave-frequency (WF) top end motions.

More details about the model can be found in Falkenberg et al. (2017) while the determination of static and dynamic stiffness is focused in this paper. The static stiffness is represented by the nonlinear working curve depending on previous highest mean tension. It describes a nonlinear relation between mean tension and mean stretch which is used to estimate the offset due to mean environmental loads. The dynamic stiffness, applied for both LF and WF load effects, is linear and increases with mean tension. The proposed models are linearly dependent on mean tension only. The analytical expression of the linearized static stiffness EA_s can be expressed as:

$$EA_s = \frac{dT_{mean}}{d\varepsilon} = a \cdot T_{mean} + b \cdot MBS \tag{6}$$

where ε is stretch, MBS is minimum breaking strength of the rope, T_{mean} is the mean tension, a and b are constants estimated from sub-rope testing. It is a linear differential equation and the solution is a nonlinear exponential relation between the mean tension and the stretch. By assuming zero mean tension for zero stretch, it can be further described as:

$$\frac{T_{mean}}{MBS} = \frac{b}{a} \cdot [exp\ (a \cdot \varepsilon) - 1] \tag{7}$$

The analytical expression of the linearized dynamic stiffness, EA_d is expressed as:

$$EA_d = \frac{dT_{dyn}}{d\varepsilon} = f \cdot T_{mean} + g \cdot MBS \tag{8}$$

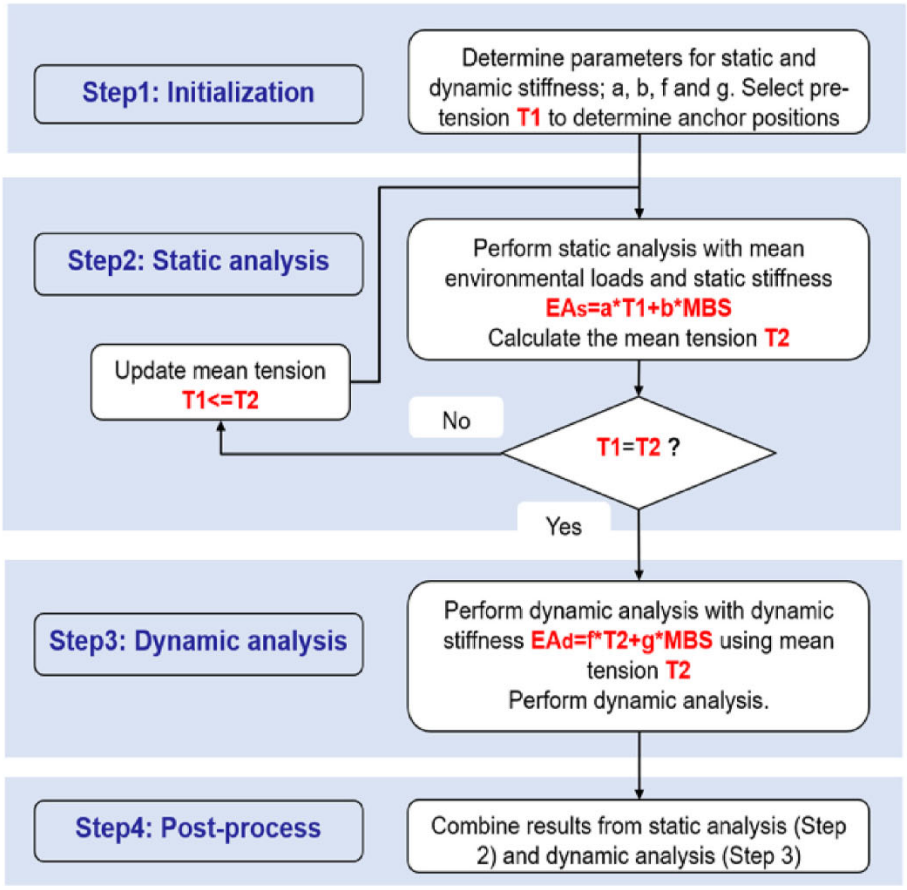

Fig. 11. Implementation of numerical analysis procedure for synthetic fibre rope in SIMA.

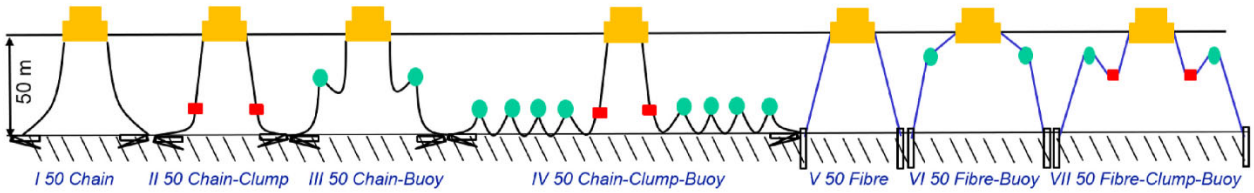

Fig. 12. Mooring configurations.

Table 2
Mooring concept introduction.

Model	Description	Feature
I	Chain	The weight is quite heavy in order to achieve reasonable pre-tension as deep water mooring.
II	Chain-Clump	Clump weight can contribute to pre-tension, so the weight of mooring line can be reduced.
III	Chain-Buoy	Buoy can influence the catenary shape by introducing more geometric stiffness.
IV	Chain-Clump-Buoy	The attachment of buoys at the resting line could help to decrease the weight of lifted line and further decrease the extreme tension at large offset.
V	Fibre	Pure synthetic fibre rope is used without any mooring components.
VI	Fibre-Buoy	Buoy is included as comparative design to include geometric stiffness.
VII	Fibre-Clump-Buoy	Both clump weight and buoy are included as comparative design.

where T_{mean} is the mean tension determined from previous static analysis using linearized static stiffness, f and g are constants estimated from sub-rope testing. Examples of linearized static and dynamic stiffness curves are given in Fig. 10.

Static stiffness is nonlinear with stretch (Equation (7)) while both static and dynamic stiffness vary with mean tension level and the mean tension is also influenced by the stiffness. Drawing lessons from Qiao and Ou (2011), the mooring analysis procedure in this paper is summarized in Fig. 11 and explained in details as follows:

Step 1: Determine the parameters of the static and dynamic stiffness models according to sub-rope testing; i.e. a, b, f and g. Initialize the mooring configuration in SIMO with prescribed mooring line properties, e.g. pre-tension, mass and length etc. Define the static stiffness based on Equation (6) with pre-tension and MBS as inputs. Thereafter, anchor positions can be determined.

Step 2: For a given sea state, perform the static analysis with mean environmental loads acting on the floater and mooring system. Calculate equilibrium position of the floater and mean tension in the lines. Update the static stiffness model (Equation (6)) with obtained mean tension until the mean tension is equal to previous iteration, which indicates that convergence is achieved.

Step 3: Based on the mean tension achieved from previous static analysis, calculate the dynamic stiffness based on Equation (8) and apply them in the final dynamic analysis of the mooring lines to document dynamic tension.

Step 4: Calculate total tension by adding the results from Step 2 and 3.

3.3. Alternative concept proposals

In view of the design criteria in Section 3.1 and the design basis in Section 3.2, seven initial mooring design concepts are proposed as shown in Fig. 12. The concepts are designed for a water depth of 50 m (shallow water) while a mooring model at 200 m (deep water) is selected as reference with respect to line length, pre-tension, offset-tension characteristics etc.

The features of the mooring models are introduced in Table 2, while the detailed properties of the mooring line are summarized in Table 3. Regarding the positions of clump weight and buoy, the mooring line which is aligned with both incoming wind-wave direction and x-z plane is taken as an example while their coordinates are given in Table 4. Among the seven designs, the first four concepts are catenary moorings using chain cable while the last three are taut moorings using synthetic fibre rope. In addition, clump weight and buoy are included in the comparative designs to check their influence on the overall performance.

The parameters of the chain is determined according to Vryhof (2015) and the parameters for the synthetic fibre rope is according to BRIDON (2013). The diameter of chain refers to the size of the steel bar, while the diameter of synthetic fibre rope refers to the size of the rope. The weight of mooring line is given as the unit weight in water. The anchor radius refers to the distance between anchor and the center of the platform. The property of buoy is given as the net buoyancy, *EAs* and

Table 4
Horizontal and vertical coordinates of clump weights and buoys in x-z plane.

Model	Component	X-coordinate	Z-coordinate
II	Clump	−103.71 m	−46.08 m
III	Buoy	−185.44 m	−33.94 m
IV	Clump	−103.7 m	−46.08 m
	Buoy	−232.41 m, −381.55 m, −530.87 m, −680.22 m	−44.02 m, −44.02 m, −44.02 m, −44.02 m
VI	Buoy	−625.89 m	−24.01 m
VII	Clump	−141.55 m	−20.37 m
	Buoy	−625.76 m	−26.52 m

Table 3
Mooring line properties.

	Material	Weight	Diameter	MBS	Length	Anchor Radius	Clump	Buoy	EAs	EAd
		kg/m	m	KN	m	m	t	KN	KN	KN
200	Chain	113.35	0.0766	6001	835.5	837.6	No	No	7.54E5	
I	Chain	613	0.175	25 174	835.5	868.8	No	No	2.62E6	
II	Chain	308	0.124	14 358	835.5	868.8	28	No	1.31E6	
III	Chain	308	0.124	14 358	835.5	868.8	No	330	1.31E6	
IV	Chain	308	0.124	14 358	935.5	965.4	28	330 × 4	1.31E6	
V	Fibre	26.5	0.203	11 772	1000	1048.9	No	No	Eq 6	Eq 8
VI	Fibre	26.5	0.203	11 772	1000	1048.9	No	70	Eq 6	Eq 8
VII	Fibre	26.5	0.203	11 772	1000	1048.9	15	70	Eq 6	Eq 8

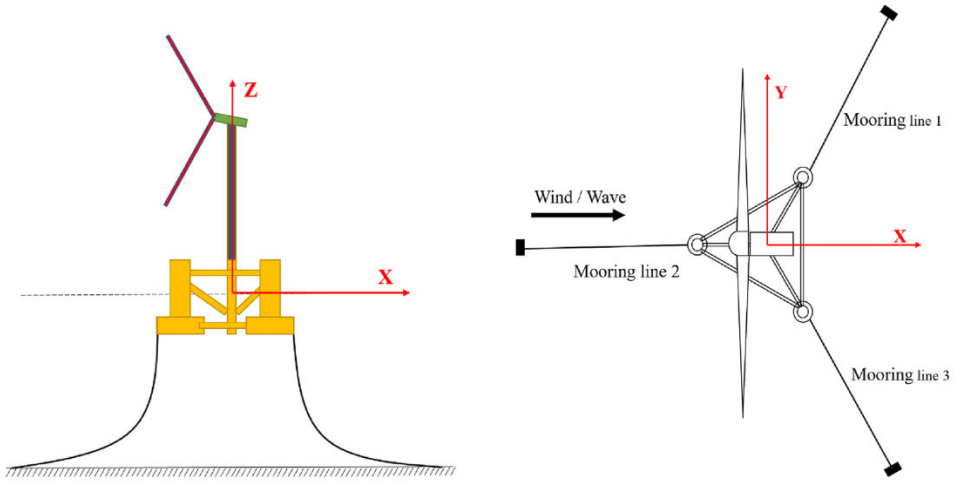

(a) Floating wind turbine (b) Mooring system

Fig. 13. OC4 Semi-submersible floating wind turbine.

Table 5
Properties of OC4 semi-submersible floating wind turbine.

Total platform draft	20 m
Elevation of tower base above still water level	10 m
Diameter of pontoons, main column	1.6 m, 6.5 m
Diameter of upper columns, base columns	12 m, 24 m
Length of upper columns, base columns	26 m, 6 m
Spacing between offset columns	50 m
Platform mass, including ballast	1.3473E7 kg
Cut-In, Rated, Cut-Out Wind speed	3 m/s, 11.4 m/s, 25 m/s
Diameter of rotor, hub	126 m, 3 m
Mass of rotor, nacelle, tower	1.1E5 kg, 2.4E5 kg, 3.47E5 kg

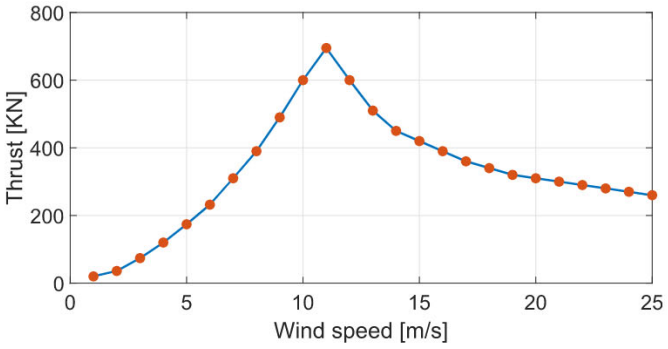

Fig. 14. Thrust curve for the 5 MW NREL wind turbine.

EAd stands for axial stiffness used in static analysis and dynamic analysis respectively as described in Equations (6) and (8).

Drag embedment anchor (DEA) is used for the four catenary mooring designs. To be more specific, 17 ton Stevshark Mk5 anchor designed by Vryhof Anchor (Vryhof, 2015) is selected. This anchor can be adjusted for varying soil conditions through modifying the shank angle. This selection is based on two reference projects: Hywind II project (Equinor, 2019) and WindFloat project (PrinciplePower, 2019) where the same anchor were used. In order to better take the vertical load from the synthetic fibre rope mooring line and achieve accurate anchor location, suction anchor is chosen for the three taut mooring designs. Similar to the conceptual TLWT project (Copple et al., 2012), a 50 ton suction anchor is chosen.

4. Case study

4.1. Floating wind turbine

In this study, the 5 MW OC4 semi-submersible wind turbine (Robertson et al., 2014) is used to compare the mooring design concepts at 50 m water depth. The semi-submersible is composed of three offset columns, three pontoons, a central column and braces. As shown in Fig. 13, the origin of the coordinate system is located at still water level, while the X-axis is the nominal wind direction, the Y-axis is lateral to the left when looking downwind and Z-axis is upward along the center line of the undisplaced platform. The mass of the floater including ballast is 1.3473E+7 kg and the dimensions of main components are listed in Table 5. The reference wind turbine mounted on top of OC4 floater is the NREL 5 MW baseline wind turbine (Jonkman et al., 2009), whose thrust curve at different wind speeds is given in Fig. 14. The mooring system is designed with three mooring lines which spread symmetrically about a vertical axis through the platform center with an angle of 120° between each line. The fairlead is located at the top of the base columns which is 14 m below the still water level. A bird view of the mooring system is given in Fig. 13 (b). Among all three mooring lines, the upwind mooring line 2 was selected as an example for the analysis later since it is aligned with the incoming wind and wave direction and subjected to the largest tension.

4.2. Load case

With the purpose of comparing the performance of different mooring design concepts, a series of representative load cases (LCs) are considered in this paper covering both operational and extreme conditions as listed in Table 6. The turbulent wind and irregular wave are correlated and directionally aligned. The LCs are selected with increasing wind speed from cut-in to cut-out wind speed with a bin size of 4 m/s while the turbulent wind field is generated according to the Norwegian Petroleum Directorate (NPD) wind spectrum. The mean wind speed U is expressed as a function of height z above mean water level:

$$U(z) = U_{ref}\left(\frac{z}{z_{ref}}\right)^{\alpha} \tag{9}$$

where U_{ref} is the reference wind speed, z_{ref} is the height of the reference wind speed and α is the power law coefficient. The reference height is set to 90 m above mean water level as the center of rotor and α was chosen to be 0.14 for floating wind turbine according to IEC 61400-3 (IEC,

Table 6
Load cases.

	U_{ref} [m/s]	T_I –	H_s [m]	T_p [s]	U_c [m/s]	Seeds –	Simulation length [s]	Turbine status
LC1	4	0.258	1.96	9.72	–	10	12 000	Operational
LC2	8	0.174	2.53	9.85	–	10	12 000	Operational
LC3	12	0.146	3.20	10.11	–	10	12 000	Operational
LC4	16	0.132	3.97	10.44	–	10	12 000	Operational
LC5	20	0.124	4.80	10.82	–	10	12 000	Operational
LC6	24	0.118	5.69	11.23	–	10	12 000	Operational
LC7	32	0.111	7.64	12.08	–	10	12 000	Parked
LC8	40	0.110	9.77	12.95	–	10	12 000	Parked
LC9	40	0.110	9.77	12.95	1.0	10	12 000	Parked

Table 7
Drag coefficients (C_d) and inertia coefficients (C_m) for different mooring line materials (DNVGL, 2018a).

	Normal C_d	Longitudinal C_d	Normal C_m	Longitudinal C_m
Stud Chain	2.6	1.4	3.1	1.7
Synthetic fibre rope	1.6	0	2	0

Table 8
Horizontal pre-tension [KN].

200 m	I	II	III	IV	V	VI	VII
914	868	910	462	859	1048	1152	1145

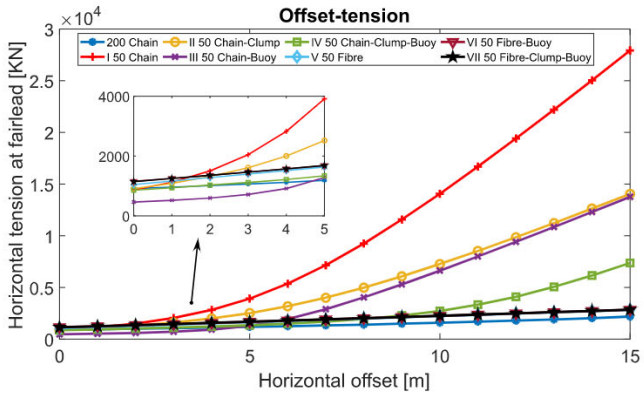

Fig. 15. Offset-tension relation for a single mooring line.

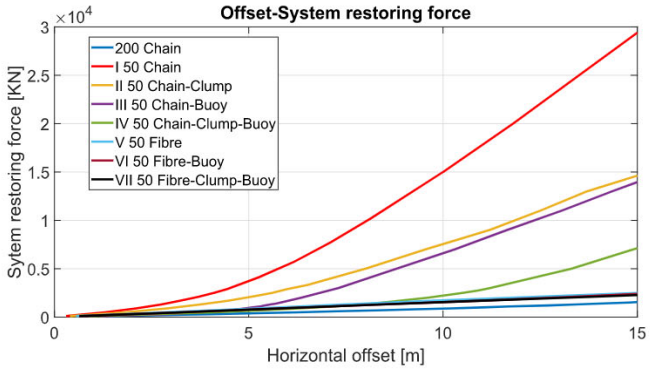

Fig. 16. System restoring force.

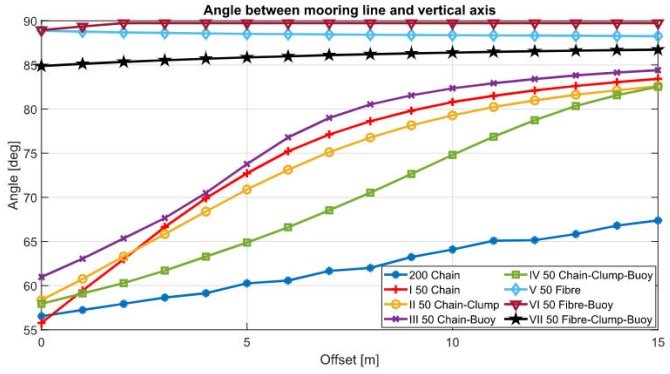

Fig. 17. Angle between mooring line and vertical plane.

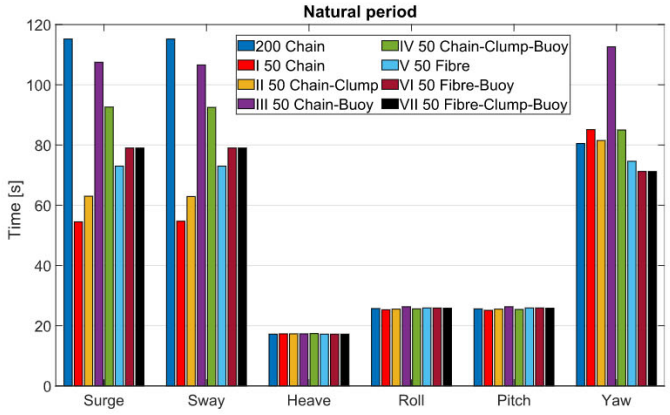

Fig. 18. Natural period.

2005). The irregular wave series are generated using JONSWAP wave model. The significant wave heights and peak periods are defined based on the correlation with wind speed for the northern North Sea (Johannessen et al., 2001). Considering a water depth of 50 m in this paper, LC8 is about same level as 50-year extreme condition at North Sea, which is sufficient for an intact ULS check for mooring system of a floating wind turbine (DNVGL, 2018b).

In addition, current load effect is accounted for in LC9 whose wind and wave condition is same as LC8. According to DNVGL–OS–E301 (DNVGL, 2018a), the current can be categorized as tidal, circulation, wind-generated, soliton and loop currents, depending on the site location. A surface current speed (U_c) with 10-year return period is recommended for mooring analysis. Based on the typical surface current speeds as given in DNVGL (2018a), 1.0 m/s is chosen as a representative surface current velocity in this paper. The variation is considered as a linear profile from still water level to $z = -50\ m$ as shown in Equation (10). The current is assumed to vanish at water depth deeper than 50 m

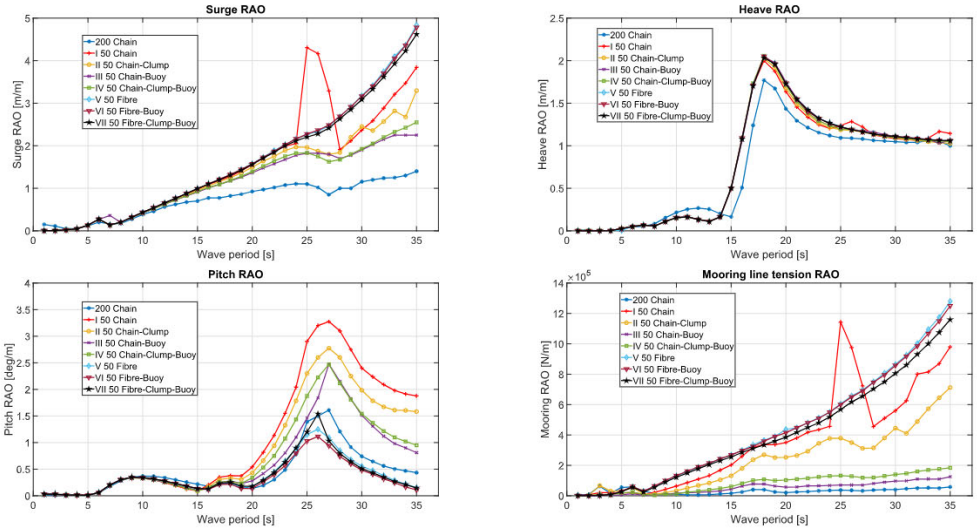

Fig. 19. Response RAO in regular wave.

Table 9
Mean horizontal environmental forces for all load cases *[KN]*.

	LC1	LC2	LC3	LC4	LC5	LC6	LC7	LC8	LC9
50 m	134.48	415.53	636.66	435.48	350.18	320.32	65.98	78.68	475.45
200 m	132.23	412.88	631.44	428.76	341.65	310.77	56.77	71.65	401.32

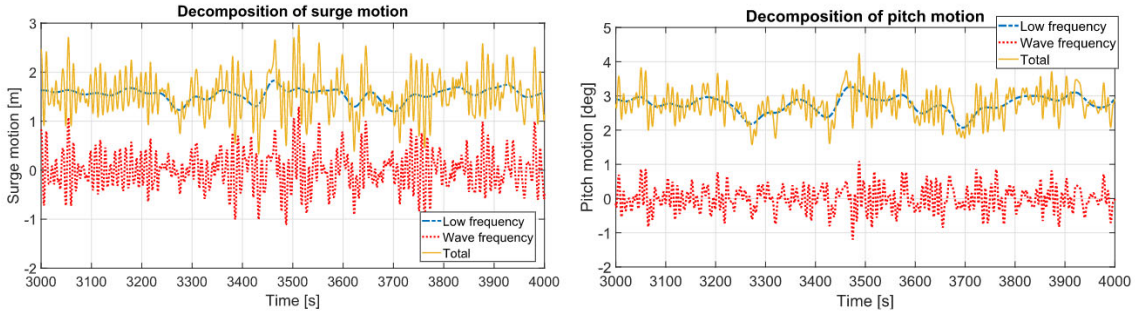

(a) Surge (b) Pitch

Fig. 20. Time series of surge and pitch motion and their WF and LF components.

and same current profile is used for both 50 m and 200 m water depth.

$$U_c(z) = 1.0 \cdot \left(\frac{50+z}{50}\right) \quad \text{for} \quad -50 \le z \le 0 \tag{10}$$

Since the focus of this paper is to demonstrate the pros and cons of different mooring design concepts rather than a sophisticated mooring system design, load cases prioritized in this paper are relevant for ULS criteria.

4.3. Fully coupled dynamic analysis

The aero-hydro-servo-elastic behaviors of the floating wind turbine systems requires sophisticated coupled dynamic analysis method. The dynamic motion equation of the floater in time domain can be written as:

$$(\mathbf{M}+\mathbf{A}_\infty)\,\ddot{\vec{r}}(t) + \int_0^t \boldsymbol{\kappa}(t-\tau)\,\dot{\vec{r}}(\tau)d\tau + \mathbf{K_s}\cdot\vec{r}(t) = \vec{T}\left(t,\vec{r},\dot{\vec{r}},\ddot{\vec{r}}\right) + \vec{q}\left(t,\vec{r},\dot{\vec{r}}\right) \tag{11}$$

where $\mathbf{M}$ is the mass matrix, $\mathbf{A}_\infty$ is the added mass matrix at infinite frequencies, $\boldsymbol{\kappa}(t-\tau)$ is the retardation function (Faltinsen, 1993) which is calculated from frequency-dependent added mass or potential damping, $\mathbf{K_s}$ is the hydrostatic restoring matrix, $\vec{r}, \dot{\vec{r}}, \ddot{\vec{r}}$ are the displacement, velocity and acceleration, $\vec{T}$ is force from mooring system, $\vec{q}$ is the external force which includes first, second order wave excitation force and wind force.

In this paper, the frequency-dependent added mass and radiation damping and first order wave forces are calculated in HydroD (DNV GL, 2016) which is a potential flow solver. The linear damping as well as quadratic damping are included based on decay test results. The second order difference-frequency wave excitation force is calculated using full quadratic transfer function (QTF) with additional meshing of the free surface. Compared with Newman's approximation method whose computation time is about several minutes, the computational effort for full QTF method is much more intensive, which takes approximately 22 h. However, full QTF method is necessary for limiting the uncertainty of heave, roll and pitch motion prediction in which Newman's

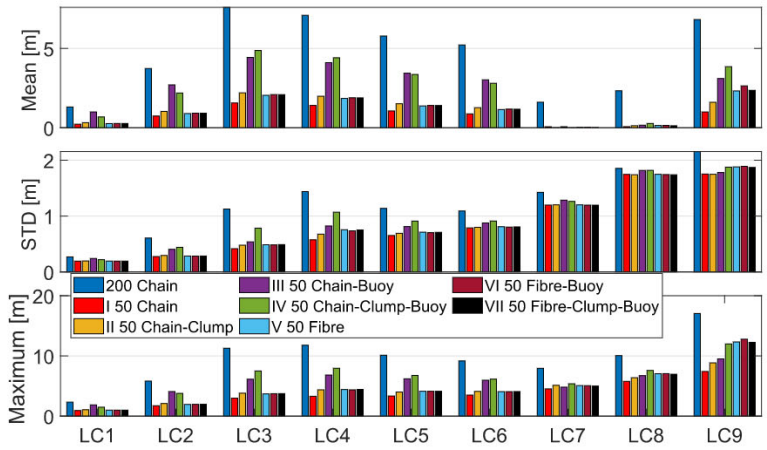

(a) Surge

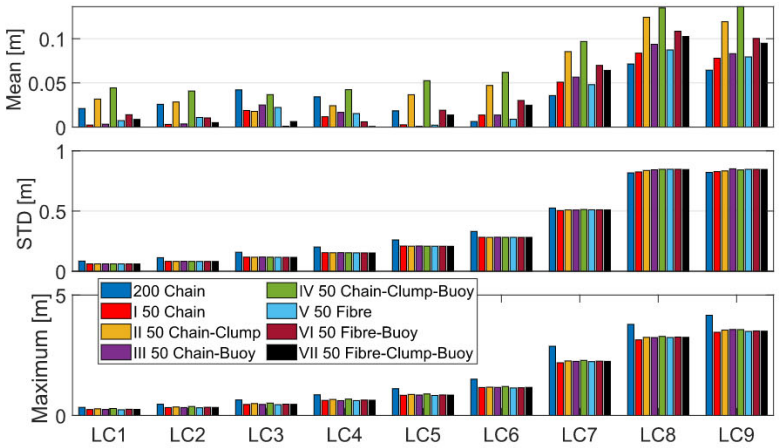

(b) Heave

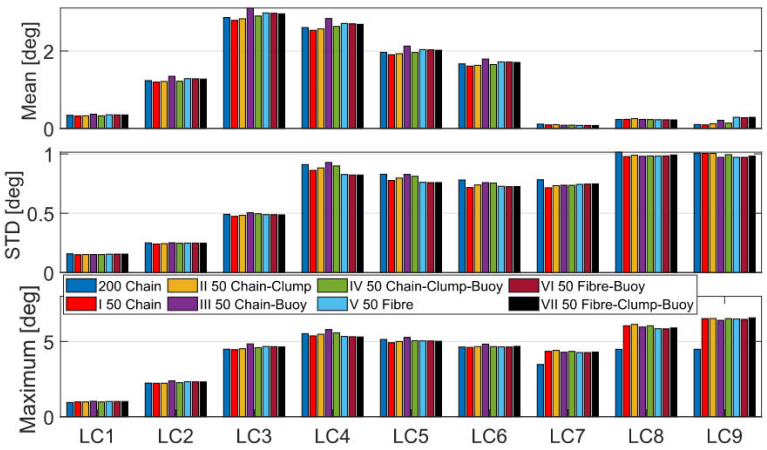

(c) Pitch

Fig. 21. Statistics of motion response.

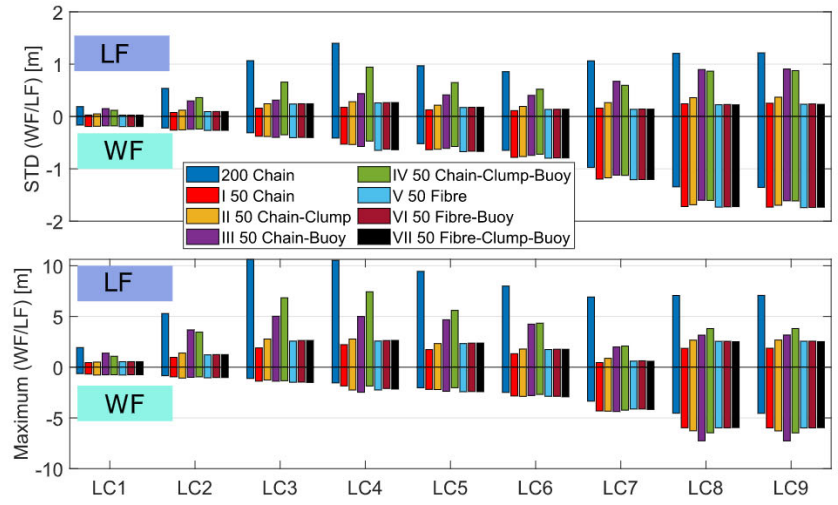

(a) Surge

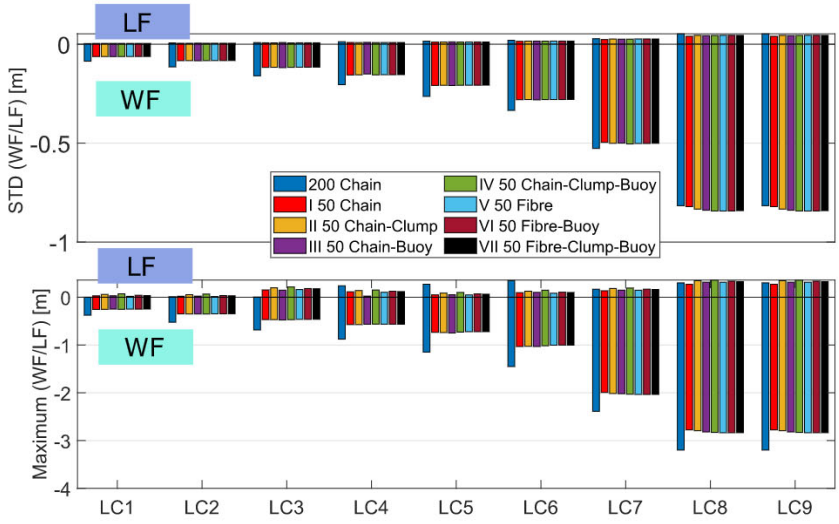

(b) Heave

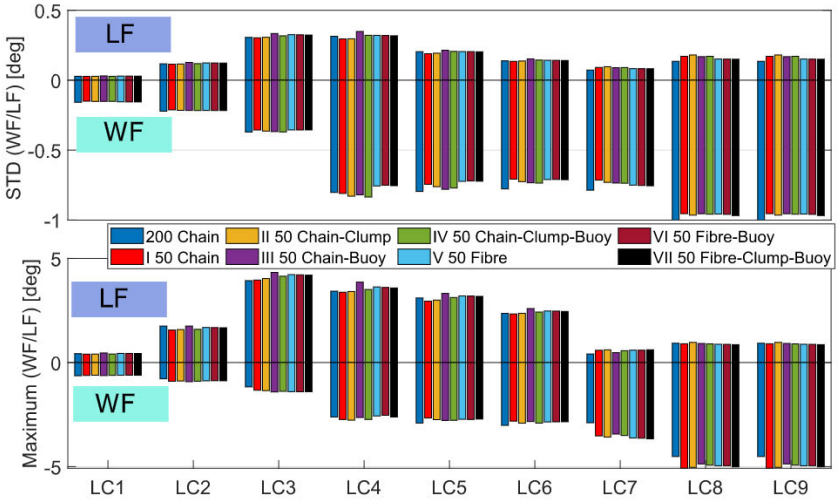

(c) Pitch

Fig. 22. Decomposition of responses into WF and LF components.

- **Surge:** The surge response for the reference model in 200 m is in general larger than all the models in 50 m. The mean value of surge motion is relatively large when wind speed is around rated wind speed (LC3) or current load is considered (LC9) while the standard deviation and maximum increase as wave becomes more and

more severe. For the seven designs in 50 m, the mean and maximum value for Model III and IV are relatively larger than others, which will directly influence the mooring line tension. LF components of standard deviation and maximum are relatively large in operational conditions while WF components are dominating in extreme conditions.

- **Heave:** The heave response increases from LC1 to LC8 for all the models as wave height increases. Meanwhile, the current effect is limited for heave responses by comparing the results for LC9 with those for LC8. No significant difference is found for different mooring models. As shown in Fig. 22 (b), heave motion is WF-dominated in all load cases.
- **Pitch:** Similar to surge motion, the mean value of pitch motion is also wind-dominated while the standard deviation and maximum increase as environmental condition becomes more severe. There is no big discrepancy from different models in all load cases even the taut mooring systems do not show any disadvantages. From Fig. 22 (c), the maximum value is dominated by LF component in operational condition and WF component in extreme condition respectively while the standard deviation mainly comes from WF component.

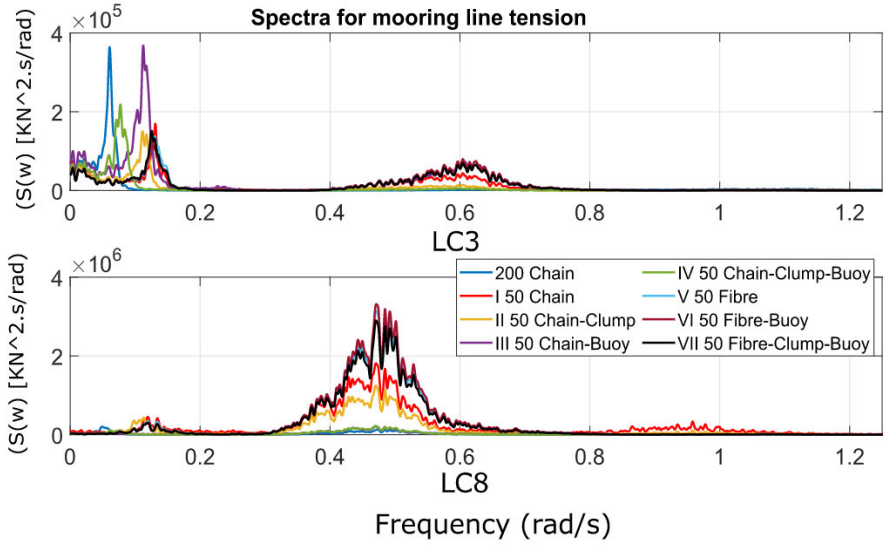

Fig. 23. Spectra for mooring line tension in LC3 and LC8.

approximation has limitation. Viscous effect on the floater is modeled by the drag term in Morison's equation and the hydrodynamic force acting on mooring line is computed using Morison's equation. Based on finite element method (FEM), the mooring line is defined in terms of sequence of segments with homogeneous cross-sectional properties. The drag coefficients for catenary chain cable and synthetic fibre rope are determined according to DNVGL–OS–E301 (DNVGL, 2018a) as shown in Table 7. Both the clump weight and buoy are modeled with separated bodies whose mass and volume are carefully calculated to achieve desired net gravity and net buoyancy. The aerodynamic load is calculated based on BEM theory with 3D wind velocity model. The time-domain simulations are perform in SIMA (SINTEF Ocean, 2018a, b). The motion equation is solved using Newmark-beta integration with time step of 0.02s.

5. Results and discussions

5.1. Static analysis

5.1.1. Pre-tension

Sufficient pre-tension prevents large floater x-offset due to mean and LF environmental load. It is influenced by the submerged weight of the suspended mooring line for catenary mooring system and initial line stretching for taut mooring system. The horizontal pre-tension for the seven designs are listed in Table 8 where the value for 200 m is set as a reference. As expected, the horizontal pre-tension for Model III is smaller compared with other models because of the buoy attached to the suspended line.

5.1.2. Offset characteristics

Mooring line tension properties with increasing in-line x-offsets at fairlead are studied in Fig. 15. According to Campanile et al. (2018), the recommended admissible floater offset to water depth ratio is 0.3 at 50 m depth, therefore the static mooring line tension characteristics is compared up to 15 m x-offset. The amplitude of typical low-frequency and wave frequency motions is in the range between 2 m and 4 m for operational conditions, while the extreme motion is just below 15 m as shown in Fig. 21. The tension for the three taut moorings increases linearly with increasing x-offset while the effect due to the implementation of clump weight and buoy is not significant, which is quite different from catenary type. As for the four catenary moorings, the tension increases linearly at small x-offsets while the increment becomes nonlinear at large x-offsets. This is a typical characteristics for catenary mooring system and it is more significant for shallow water (50 m) than deep water (200 m) (Xu et al., 2018). Among the four catenary moorings, the nonlinear increment of Model I is the most noticeable due to large unit weight while Model IV is the least noticeable thanks to the buoy attached at the resting line. The performance of Model IV, V, VI, VII are quite close to the reference model 200 m.

As a reference, the total horizontal mooring system restoring forces with respect to increasing horizontal x-offsets are given in Fig. 16. It will provide a general idea of mean horizontal motion when exposed to mean environmental loads as well as the range of total restoring force due to WF and LF motion.

5.1.3. Vertical angle

The issue regarding the angle between mooring line and vertical axis has been introduced in Section 2. The change of the angle α (as shown in Fig. 5) with increasing x-offset at fairlead is shown in Fig. 17. Since the water depth is quite small (50 m) compared with mooring line footprint (about 900 m), the stretched synthetic fire rope mooring line is almost parallel to the seabed with angle close to 90°, while the influence of

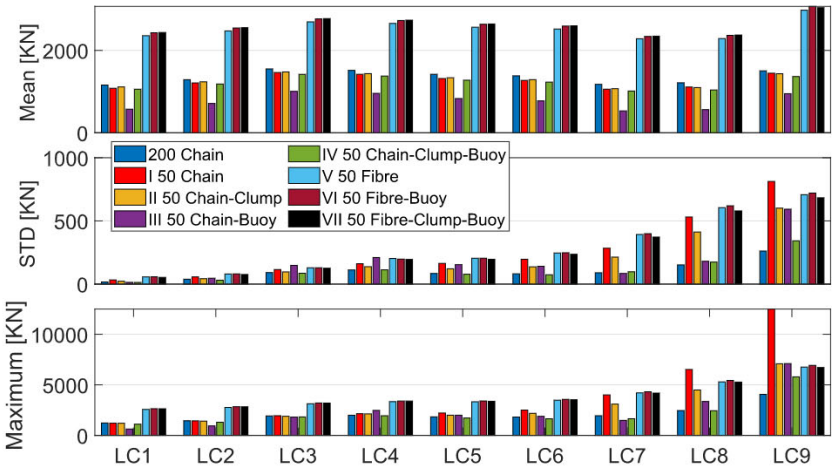

(a) Statistics of mooring line tension

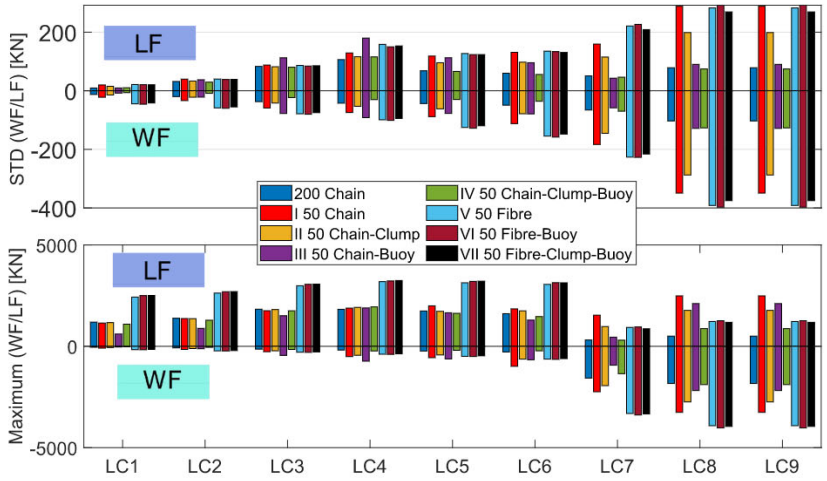

(b) Decomposition of mooring line tension into WF and LF components

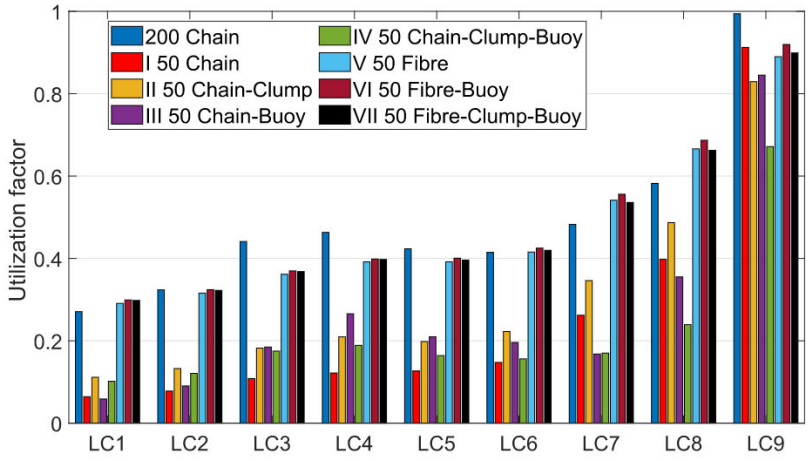

(c) Mooring line tension utilization factor

Fig. 24. Mooring line tension response.

Table 10
Price for chain, steel wire rope and synthetic fibre rope (€/N).

	Chain	Steel wire rope	Synthetic fibre rope
Price	0.25	0.5	0.7

adding clump weight and buoy is quite limited. As for the four catenary moorings in 50 m, the initial angles are around 60°, indicating a significant catenary shape. As x-offset increases, the angles starts to approach 90° indicating the loss of catenary shape and the likely stretching of the line. Better performance is achieved by Model IV because of the application of buoys. Meanwhile, the angle problem is not significant for the catenary mooring in 200 m.

5.2. Decay analysis

Prior to the dynamic analysis, it is important to check the natural periods of the semi-submersible which is greatly influenced by the mooring system characteristics in horizontal plane (surge, sway and yaw). Free decay test in calm water were performed to compare the natural periods for the different concepts and the final results are summarized in Fig. 18. The natural periods in heave, roll and pitch degrees of freedom are barely influenced by mooring system which is as expected. The reference natural period (surge, sway and yaw) for water depth 200 m is larger than all the designs in 50m. Additionally, larger periods are found for Model III which indicates that buoy will reduce the restriction of the system. The natural period for Model V is smaller than Model VI and VII, because the application of clump weight and buoy will include more geometric stiffness.

5.3. Dynamic analysis

5.3.1. Regular wave

The hydrodynamic characteristics of the mooring concepts are further compared by response amplitude operator (RAO), which are determined through a number of regular wave simulations. Since wave nonlinearity characterized by the ratio between wave amplitude and wave period will affect the RAO analysis, the amplitude of the regular wave in this paper is chosen to be 1 m and wave period ranges from 1 s to 35 s in order to cover most probable excitation wave components. The motion reference point is taken as the origin of the coordinate system which is located at the mean water level. Floater motions such as surge, heave, pitch and mooring line tension are studied in Fig. 19.

The theoretical asymptomatic behavior of surge motions for freely floating structures in long waves tends to follow the elliptical trajectory of water particles at finite water depth. The amplitude of the horizontal motion of the water particles in shallow water can be written as: $A/tanh(kh) \approx A/kh$, where A is wave amplitude, k is wave number and h is water depth. Accordingly, given the same wave amplitude, the motion amplitude will increase as water depth decreases. Therefore in this study, the surge RAOs for all the moorings in 50 m are larger than the reference model in 200 m. The coupling between surge and pitch results in the large surge RAO peak at pitch natural frequency which is more significant for catenary moorings than taut moorings. In addition, the RAOs are not greatly influenced by mooring systems for the range of wave periods from 5 s to 15 s. As a result, the wave frequency motions are not influenced by the mooring system when exposed to irregular waves, which is as expected. However, as for low frequency motions, in particular the resonant pitch motions around 25 s and the associated surge motions are strongly influenced by the mooring system. The heave RAO is almost the same for all the moorings in 50 m which proves again that floater heave motion is almost not affected by mooring system. Pitch resonance leads to the largest pitch RAO peak and apparent difference are found for different mooring concepts because of different stiffness. The mooring line tension RAO is directly influenced by floater horizontal motion, therefore, the surge RAO peak due to pitch resonance also result in a peak of mooring line tension RAO. There is a significant difference in the mooring line tension RAO in the range of wave periods from 5 s to 15 s, which will influence the dimension of the mooring lines. In realistic sea state where nonlinear mooring line tension behavior becomes more significant, the tension RAO curve presented here may lead to underestimation compared with dynamic analysis result in high sea state.

5.3.2. Irregular wave and turbulent wind

The environmental parameters are given in Section 4.2. Six operational conditions where turbine is rotating and three extreme conditions where turbine is parked are defined in order to compare the mooring performance. The results are achieved for 3 h response by running each simulation for 12 000 s while the first 1200 s is excluded because of

Table 12
Summary of Pros and Cons for all mooring concepts.

No	Model	Pors and Cons	Recommend for further assessment
I	Chain	Mooring line is quite heavy, the extreme mooring line tension is quite large and the cost is very high.	NO
II	Chain-Clump	Clump weight can contribute to pre-tension, but line tension in extreme condition is not improved. The cost is lower than pure chain cable mooring.	**YES**
III	Chain-Buoy	Buoy can reduce the extreme tension, but it will decrease the pre-tension. The reduction of extreme tension is not significant.	**YES**
IV	Chain-Clump-Buoy	The merits of clump weight and buoy are included. The extreme tension at large offset is avoided. The cost is competitive thanks to lower utilization.	**YES**
V	Fibre	Desired pre-tension is much easier to achieve than catenary mooring. The tension increment is linear even for large offset. The cost is acceptable considering its performance.	**YES**
VI	Fibre-Buoy	The effect of adding extra buoy to synthetic fibre rope is quite limited.	**YES**
VII	Fibre-Clump-Buoy	The effect of adding buoy and clump weight to synthetic fibre rope is not significant.	**YES**

Table 11
Cost breakdown for mooring system (€).

	Anchor	Line	u	Clump	Buoy	Installation	Total
200 m	114k × 3	236.8k × 3	0.994	0	0	55k × 3	**1.21m**
I	114k × 3	1280.4k × 3	0.912	0	0	55k × 3	4.01m
II	114k × 3	643.3k × 3	0.829	70k × 3	0	55k × 3	2.32m
III	114k × 3	643.3k × 3	0.875	0	1.3k × 3	55k × 3	2.20m
IV	114k × 3	720.3k × 3	0.671	70k × 3	1.3k × 4*3	55k × 3	**2.18m**
V	512.5k × 3	185.5k × 3	0.889	0	0	88k × 3	**2.30m**
VI	512.5k × 3	185.5k × 3	0.920	0	0.8k × 3	88k × 3	2.31m
VII	512.5k × 3	185.5k × 3	0.898	37.5k × 3	0.8k × 3	88k × 3	2.41m

transient effect. 10 different realisations of turbulent wind and irregular wave are generated for each load case to account for the stochastic variability. The expected maximum of the response is determined as the average of the 10 individual sample maxima. Floater motions and windward line are selected as representative responses in this section. The mean horizontal environmental forces including mean wind force and second-order wave force for all the load cases are given in Table 9. The mean environmental force in LC9 is significantly larger than that in LC8 due to the current load effect. The mean, standard deviation and maximum of the floater motion in surge, heave and pitch directions are provided for each load case in Fig. 21. In addition, the total response is also decomposed into WF and LF components for comparison. An example of time series for surge motion in LC3 is given in Fig. 20 consisting of total motion, WF motion and LF motion. As the mean value of WF response is around zero, therefore only the standard deviation and maximum are compared in Fig. 22 with LF value shown above x-axis and WF value shown below x-axis.

The power spectrum of the mooring line 2 (Fig. 13) as the most loaded line, is studied in Fig. 23 with respect to the power spectra. Two representative load cases are focused: one for operational condition (LC3) and one for extreme condition (LC8). In LC3 where wind effect is strong and wave condition is not severe, low-frequency responses contributes more to the total tension response compared with wave-frequency response component. Meanwhile, in the parked condition LC8, the wind load effect is limited and the wave condition is quite severe, wave-frequency tension is governing the total response.

The statistics of mooring line tension is compared in Fig. 24 (a). The mean tensions for Model I II and IV are quite close while smaller value for Model III and larger value for Model V VI VII are observed for all the load cases. Noticeable standard deviation and maximum is found for Model I compared with others in LC9. Similar surge motion leads to quite different maximum mooring line tension in extreme condition is the best prove of different mooring line behaviors when exposed to same environmental condition. Among the four catenary designs, smaller extreme tension is obtained for Model IV thanks to the implementation of buoy. As for the three taut moorings, the extreme tensions are slightly higher than the catenary moorings. This is valid for the level of elastic stiffness that is used in this paper. There is a need for synthetic fibre ropes with lower elastic stiffness properties for effective mooring of floating wind turbines, especially in shallow water. The tension responses for LC9 is larger than that for LC8 due to the current load effect. From Fig. 24 (b), LF component is dominating in operational condition while WF component is governing in extreme condition.

Considering different capacity associated with different mooring materials, utilization factor recommended by DNVGL-ST-0119 (DNVGL, 2018b) can provide another perspective of tension responses to their material limit apart from the direct comparison of the statistics. The utilization factor u is defined as:

$$u = \frac{T_{pret}\gamma_{pret} + T_{C-env}\gamma_{env}}{S_C} \tag{12}$$

where T_{pret} is the mooring line pre-tension, T_{C-env} is the characteristic environmental tension due to mean, low-frequency and wave-frequency load which is calculated as $T_{MPM} - T_{pret}$, where T_{MPM} is the most probable maximum tension, S_C is the characteristic mooring line strength defined as 95% of the minimum breaking strength S_{MBS}, γ_{pret} and γ_{env} are safety factors which are set as 1.3 & 1.75 respectively in this paper based on the assumption of level 1 consequence class.

The resulting utilization factors for all the models in all load cases are shown in Fig. 24 (c). First of all, all the utilization factors are below 1 which means the line capacities are not exceeded for all the models and they are close to 1 in the most extreme condition meaning that line redundancy is within acceptable range. In operational conditions where the tension level is small, the utilization factors for taut moorings are slightly larger than catenary moorings. However in extreme conditions when the tension level is high, the utilization factors for catenary moorings increase dramatically compared with taut moorings. Speaking of individual mooring performance, almost no difference is found among Model V VI VII and clearly better performance is found for Model IV.

5.4. Cost analysis

Economic consideration plays an important role in the mooring decision. The expense of an offshore wind project can be evaluated by capital expenditures (CAPEX) or operating expenditures (OPEX) (Myhr et al., 2014). When a complete time span is considered for different phases of the project, life cycle cost analysis (LCCA) is preferred for evaluation. Since the focus of this paper is to compare different mooring design concepts for the same floating wind turbine, the LCCA analysis will focus on the mooring system rather than the whole wind turbine. In addition, the comparison is performed mainly for manufacture and installation in LCCA. It is worth noticing that the cost related to maintenance and repair could be different.

It is well known that estimation of the mooring expense is not a simple task due to the lack of publicly available data. The costs of mooring line, anchor and installation etc. have been investigated by several researchers (Campanile et al., 2018; Myhr et al., 2014; Andreas and John, 2012; Bjerkseter and Ågotnes, 2013; Klingan, 2016; Audibert et al., 2003; Benassai et al., 2015; Fylling and Berthelsen, 2011), which are mainly preliminary studies. In this paper, an elementary cost analysis is also performed based on some of the references mentioned and the main purpose is to provide a general cost-wise ranking of the seven mooring designs. The total cost also takes into account the utilization factor of mooring line.

The detailed anchor capacity design is not the focus of this paper, therefore anchors from well-proven industrial projects are referred. According to Bjerkseter and Ågotnes (2013), the price of a 17 ton Stevshark Mk5 anchor from Vryhof Anchors is approximately €114000, while a 50 ton suction anchor costs around €512500.

The price for mooring line is estimated according to the objective function in Klingan (2016) which is based on data provided by Equinor. The prices for chain, synthetic fibre rope and steel wire basically can be described by a common expression with different coefficients.

$$Cost = Length * Weight * Price \tag{13}$$

where length is given in m, weight in the air is given in N/m and the price is given in $€/N$ for different materials as shown in Table 10.

The price for two clump weights are estimated as heavy chain using Equation (13) while the price for two buoys are estimated using data from Defender (2019) with a linear interpolation.

The installation procedure for all the models in this paper is assumed to be performed by one large anchor handling tug supply vessel with sufficient holding capacity. According to Audibert et al. (2003), the installation time for a DEA anchor is about 8 h including deck rigging, launching, lowering, seabed penetrating and tensioning while it takes about 12 h to install a suction anchor including seabed penetrating and deck handling. Combining other assumptions as shown in Bjerkseter and Ågotnes (2013), the baseline mooring system installation costs for all concepts are obtained.

The total cost for all the mooring models are calculated in Table 11 by summing up the manufacture and installation costs. The price is listed in Euro (€), k stands for 10^3 and m stands for 10^6. u indicates the maximum utilization factor of the mooring line in LC9 as shown in Fig. 24. Generally, the catenary mooring is competitive regarding the cost of anchor and installation but the capital cost for the mooring line is quite high. The taut mooring on the other hand is favorable with respect to the cost of synthetic fibre rope, however the cost for the suction anchor and installation is quite high. Clearly, the cost of the reference model in 200 m is quite low compared with the models in 50 m since the cost of the mooring line is low. Model I is the most expensive model

because of the high price for the heavy chain. Model IV and V are more cost-competitive designs of their types, while the difference with other models is not significant. Meanwhile, current cost estimates are based on ULS design criteria and certain number can be different if FLS and ALS design check are respected too. In addition, the cost estimation in this paper can be subject to variations given particular project, location, timing and supplier. Therefore, Model II–VII are all recommended for further assessment.

6. Conclusions

In order to further promote the industrial development of offshore floating wind turbine, the challenges and solutions regarding mooring system design in shallow water is systematically studied in this paper. Seven mooring design concepts for OC4 semi-submersible floating wind turbine are proposed at 50 m water depth. Different mooring line materials and mooring components are used. The comparative designs are proposed by taking full advantage of both geometric and elastic mooring stiffness. The stiffness characteristics for synthetic fibre rope is described with an improved numerical model based on latest experimental data. The concepts are evaluated through static, decay, dynamic and cost analysis. Finally, two mooring concepts with better performance and competitive cost are recommended for future application.

The geometric effect is the most important parameter for catenary mooring at shallow water. Clever inclusion of heavy chain or clump weight have to be used in order to achieve a reasonable pre-tension and stiffness characteristics. The nonlinearity in the line characteristics is pronounced for traditional catenary systems, which can be improved by smart use of buoys and/or clump weights. The use of synthetic fibre ropes instead of chain cable will also reduce the nonlinear characteristics, but the benefit of including clump weight and buoy is not significant. From dynamic analysis, the extreme tension for pure chain mooring is extraordinarily large compared with other concepts. Judging from the mooring utilization factor, hybrid catenary mooring (Model IV) clearly stands out. From the cost analysis, the capital cost of mooring chain is high while the cost of its DEA anchor and installation is relatively low. On the contrary, the cost of synthetic fibre rope mooring line is quite low, however the cost for the suction anchor and installation is quite high. When combining with the utilization factor, Model IV and V are cost-competitive concepts. The advantages and disadvantages of the seven mooring designs are further summarized in Table 12.

In conclusion, taking the structural performance and capital cost of different models into account, model II–VII are all recommended for further assessment related to floating wind mooring design in shallow water in the future. As for the future work, the proposed mooring concepts need to be further verified with fatigue analysis and accidental analysis. More load cases including the current effect is also of interest to consider.

CRediT authorship contribution statement

Kun Xu: was responsible for initiating ideas, Formal analysis, Writing – original draft. **Kjell Larsen:** provided important knowledge regarding the experimental data and numerical analysis procedure of synthetic fibre rope. **Yanlin Shao:** offered insight of industrial application of synthetic fibre rope mooring system. **Min Zhang:** contributed with constructive discussions, corrections and comments to increase the quality of the publication. **Zhen Gao:** contributed with constructive discussions, corrections and comments to increase the quality of the publication. **Torgeir Moan:** contributed with constructive discussions, corrections and comments to increase the quality of the publication.

Declaration of competing interest

The authors declare that they have no known competing financial interests or personal relationships that could have appeared to influence the work reported in this paper.

Acknowledgement

The first author would like to acknowledge the financial support from China Scholarship Council (201607950005). The authors would like to thank Equinor for sharing the information regarding modelling of synthetic fibre rope. The valuable discussion with Tiril Stenlund from 7 Waves AS is appreciated.

References

4COffshore, 2020. Fourth kincardine foundation on the move. URL. https://www.4coffshore.com/news/fourth-kincardine-foundation-on-the-move-nid17134.html.
Andreas, B.P., John, F.I., 2012. Conceptual design of a floating support structure and mooring system for a vertical axis wind turbine. In: ASME 31st International Conference on Ocean, Offshore and Arctic Engineering. American Society of Mechanical Engineers (ASME), Rio de Janeiro, Brazil.
API, 2014. API-RP-2SM Design, Manufacture, Installation, and Maintenance of Synthetic Fiber Ropes for Offshore Mooring.
Audibert, J.M., Clukey, E., Huang, J., et al., 2003. Suction caisson installation at horn mountain–a case history. In: The Thirteenth International Offshore and Polar Engineering Conference. International Society of Offshore and Polar Engineers.
Benassai, G., Campanile, A., Piscopo, V., Scamardella, A., 2014a. Mooring control of semi-submersible structures for wind turbines. Procedia Engineering 70, 132–141.
Benassai, G., Campanile, A., Piscopo, V., Scamardella, A., 2014b. Ultimate and accidental limit state design for mooring systems of floating offshore wind turbines. Ocean. Eng. 92, 64–74.
Benassai, G., Campanile, A., Piscopo, V., Scamardella, A., 2015. Optimization of mooring systems for floating offshore wind turbines. Coast Eng. J. 57.
Bjerkseter, C., Ågotnes, A., 2013. Levelised Costs of Energy for Offshore Floating Wind Turbine Concepts. Master's thesis. Norwegian University of Life Sciences, Ås.
BRIDON, 2013. Oil and Gas, Wire and Fibre Rope Solutions for the World's Most Demanding Applications. Technical Report. BRIDON.
Brommundt, M., Krause, L., Merz, K., Muskulus, M., 2012. Mooring system optimization for floating wind turbines using frequency domain analysis. Energy Procedia 24, 289–296.
Bugg, D.L., Vickers, D., Dorchak, C., 2004. Mad dog project: regulatory approval process for the new technology of synthetic (polyester) moorings in the gulf of Mexico. In: Offshore Technology Conference 16089.
Campanile, A., Piscopo, V., Scamardella, A., 2018. Mooring design and selection for floating offshore wind turbines on intermediate and deep water depths. Ocean. Eng. 148, 349–360.
Carnegie Clean Energy, 2020. Ceto next generation. URL. https://www.carnegiece.com.
Copple, R.W., Capanoglu, C., et al., 2012. Tension leg wind turbine (TLWT) conceptual design suitable for a wide range of water depths. In: The Twenty-Second International Offshore and Polar Engineering Conference. International Society of Offshore and Polar Engineers.
Defender, 2019. The marine outfitter of choice for boating enthusiasts since 1938. URL. https://www.defender.com/.
DNV GL, 2016. HydroD User Manual.
DNVGL, 2015. DNVGL-RP-E305 Design, Testing and Analysis of Offshore Fibre Ropes.
DNVGL, 2018a. DNVGL-OS-E301 Position Mooring.
DNVGL, 2018b. DNVGL-ST-0119 Floating Wind Turbine Structures.
edp renewable, 2020. Windfloat atlantic project starts supplying clean energy in Portugal. URL. https://www.edpr.com/en/news/2020/01/02/windfloat-atlantic-project-starts-supplying-clean-energy-portugal.
Equinor, 2019. Equinor - the world's leading floating offshore wind developer. URL. https://www.equinor.com/en/what-we-do/hywind-where-the-wind-takes-us.html.
Equinor, 2020. Statoil to build the world's first floating wind farm: Hywind scotland. URL. https://www.equinor.com/en/news/hywindscotland.html.
Falkenberg, E., Åhjem, V., Yang, L., et al., 2017. Best practice for analysis of polyester rope mooring systems. Offshore Technology Conference. Housten Texas.
Faltinsen, O.M., 1993. Sea Loads on Ships and Offshore Structures, 1. Cambridge university press.
Finn, L., 1976. A new deepwater offshore platform - the guyed tower. In: Offshore Technology Conference. Houston, Texas.
Fitzgerald, J., Bergdahl, L., 2007. Considering mooring cables for offshore wave energy converters. In: 7th European Wave Tidal Energy Conference. Porto, Portugal.
Fylling, I., Berthelsen, P.A., 2011. Windopt: an optimization tool for floating support structures for deep water wind turbines. In: ASME 2011 30th International Conference on Ocean, Offshore and Arctic Engineering. Rotterdam, The Netherlands.
Gaertner, E., Rinker, J., Sethuraman, L., Zahle, F., Anderson, B., Barter, G.E., Abbas, N.J., Meng, F., Bortolotti, P., Skrzypinski, W., et al., 2020. IEA Wind TCP Task 37: Definition of the IEA 15-Megawatt Offshore Reference Wind Turbine. Technical Report. National Renewable Energy Lab.(NREL), Golden, CO (United States).
Global Wind Energy Council, 2019. Global Wind Report 2018. Brussels, Belgium.
ideol, 2020. France's first offshore wind turbine and ideol's first demonstrator. URL. https://www.ideol-offshore.com/en/floatgen-demonstrator.
IEC, 2005. IEC 61400-1: wind turbines part 1: design requirements. International Electrotechnical Commission.

INNWIND.EU, 2017. Deliverable D4.3.7 Design Solutions for 10MW Floating Offshore Wind Turbines.
Johannessen, K., Meling, T.S., Haver, S., et al., 2001. Joint distribution for wind and waves in the northern north sea. In: The Eleventh International Offshore and Polar Engineering Conference. International Society of Offshore and Polar Engineers.
Jonkman, J., Butterfield, S., Musial, W., Scott, G., 2009. Definition of a 5-MW Reference Wind Turbine for Offshore System Development.
Klingan, K.E., 2016. Automated Optimization and Design of Mooring Systems for Deep Water. Master's thesis. NTNU.
LIFES50+, 2018. Deliverable D4.5 State-Of-The-Art Models for the Two LIFES50+ 10MW Floater Concepts.
Mavrakos, S.A., Chatjigeorgiou, J., 1997. Dynamic behaviour of deep water mooring lines with submerged buoys. Comput. Struct. 64, 819–835.
Mavrakos, S., Papazoglou, V., Triantafyllou, M., Hatjigeorgiou, J., 1996. Deep water mooring dynamics. Mar. Struct. 9, 181–209.
Morrison, B.G., Asce, A.M., 1983. Guyed tower with dynamic mooring properties. J. Struct. Eng. 109, 2578–2590.
Myhr, A., Bjerkseter, C., Ågotnes, A., Nygaard, T.A., 2014. Levelised cost of energy for offshore floating wind turbines in a life cycle perspective. Renew. Energy 66, 714–728.
NS ENERGY, 2020. Kincardine floating offshore wind farm, scotland. URL. https://www.nsenergybusiness.com/projects/kincardine-floating-offshore-wind-farm-scotland/.
PrinciplePower, 2019. Windfloat. URL. http://www.principlepowerinc.com/en/windfloat.
Qiao, D., Ou, J., 2011. Comparative analysis on dynamic characteristics of deepwater hybrid mooring line. J. Ship Mech. 15.
Robertson, A., Jonkman, J., Masciola, M., Song, H., Goupee, A., Coulling, A., Luan, C., 2014. Definition of the Semisubmersible Floating System for Phase II of OC4. Technical Report. National Renewable Energy Lab.(NREL), Golden, CO (United States).
Rossi, R., Del Vecchio, C.J., Goncalves, R.C.F., 2010. Moorings with polyester ropes in petrobras: experience and the evolution. In: Offshore Technology Conference 20845.
Rowley, D.S., Leite, S., 2011. What if scenario testing of synthetic fibre rope for deepwater mooring systems. In: Offshore Technology Conference.
SINTEF Ocean, 2018a. RIFLEX 4.14.0 User Guide.
SINTEF Ocean, 2018b. SIMO 4.14.0 User Guide.
Stenlund, T., 2018. Mooring System Design for a Large Floating Wind Turbine in Shallow Water. Master's thesis. NTNU.
Vicente, P.C., Falcal, A.F.de O., Justino, P.A., 2011. Slack-chain mooring configuration analysis of a floating wave energy converter. In: Proceeding of 26th International Workshop on Water Waves and Floating Bodies. Athens, Greece.
Vryhof, 2015. Vryhof Manual - the Guide to Anchoring.
Weller, S., Johanning, L., Davies, P., Banfield, S., 2015. Synthetic mooring ropes for marine renewable energy applications. Renew. Energy 83, 1268–1278.
Wise, A.S., Bachynski, E.E., 2020. Wake meandering effects on floating wind turbines. Wind Energy 23.
Xu, K., Gao, Z., Moan, T., 2018. Effect of hydrodynamic load modelling on the response of floating wind turbines and its mooring system in small water depths. In: Journal of Physics: Conference Series. IOP Publishing., 012006.
Yuan, Z.M., Incecik, A., Ji, C., 2014. Numerical study on a hybrid mooring system with clump weights and buoys. Ocean. Eng. 88, 1–11.